Acoustic flows in a slightly rarefied gas

Nicholas Z. Liu, Daniel R. Ladiges, Jason Nassios, and John E. Sader

Phys. Rev. Fluids **5**, 043401 — Published 6 April 2020

DOI: 10.1103/PhysRevFluids.5.043401

Acoustic flows in a slightly rarefied gas

Nicholas Z. Liu[1], Daniel R. Ladiges[2], Jason Nassios[3] and John E. Sader[1*]
[1] *ARC Centre of Excellence in Exciton Science, School of Mathematics and Statistics, The University of Melbourne, Victoria 3010, Australia*
[2] *Center for Computational Sciences and Engineering, Lawrence Berkeley National Laboratory, Berkeley, California 94720, USA*
[3] *Centre of Policy Studies, Victoria University, 300 Flinders St, Melbourne, VIC 3000 Australia*

(Dated: February 13, 2020)

The Boltzmann equation provides a rigorous description of gas flows at all degrees of gas rarefaction. Asymptotic analyses of this equation yields valuable insight into the physical mechanisms underlying gas flows. In this article, we report an asymptotic analysis of the Boltzmann-BGK equation for a slightly rarefied gas when the acoustic wavelength is comparable to the macroscopic characteristic length scale of the flow. This is performed using a three-way matched asymptotic expansion, which accounts for the Knudsen layer, the viscous layer and the outer Hilbert region—these are separated by asymptotically disparate length scales. Transport equations and boundary conditions for these regions are derived. The utility of this theory is demonstrated by application to three problems: (1) flow generated by uniformly heating two plates, (2) oscillatory thermal creep induced between two plates, and (3) the flow generated by an oscillating sphere. Comparisons to numerical simulations of the Boltzmann-BGK equation and previous asymptotic theories (for long wavelength) are performed. The present theory is distinct from previous asymptotic analyses that implicitly assume long or short acoustic wavelength. This theory is expected to find application in the design and characterisation of nanoelectromechanical devices, which often generate acoustic oscillatory flows of a rarefied nature.

* Corresponding author. Email: jsader@unimelb.edu.au

I. INTRODUCTION

Sound propagation in a gas is a compressible flow phenomenon that is conventionally studied using either the inviscid Euler equations, or (less frequently), the Navier-Stokes equations that account for the effects of viscosity. These theoretical treatments provide an approximation to the non-equilibrium nature of these gas flows, that have found significant use in a host of applications. For example, they have been used to study the effects of sound waves on rocket propellant combustion [1], acoustic characterization of duct systems [2], and the acoustics of flow around rotors [3]. The effect of sound waves is also important in oscillatory systems such as in inkjet print heads [4], industrial swirled combustion [5], and magnetohydrodynamic waves [6]. The validity of these theoretical approaches is contingent on the nature of the flows, which require (i) the gas mean free path to be much smaller than the characteristic length scale over which the flow varies, e.g., the sphere radius for flow over a sphere, and (ii) that the molecular collision time is far greater than any macroscopic time scale of the flow. This leads to the well-known constraints:

$$\mathrm{Kn} \equiv \frac{\lambda}{L} \ll 1, \qquad \theta \equiv \frac{\omega}{\nu} \ll 1, \tag{1}$$

where Kn is the Knudsen number, λ is the mean free path, L is the macroscopic length scale of the flow, θ is the frequency ratio, ω is the macroscopic oscillation frequency, and ν is the collision frequency.

Two common situations give rise to gas flows with non-vanishing Knudsen number. First, low gas density flows, which naturally occur in the upper atmosphere, obviate use of the above-mentioned continuum treatments. Applications include the aerodynamics of atmospheric re-entry [7] and the drag experienced by low Earth orbit satellites [8]. Second, gas flows generated by devices of size comparable to the gas mean free path at atmospheric temperatures and pressures, e.g., resonant nanoelectromechanical systems that naturally generate oscillatory flows [9]. Violation of the second condition in Eq. (1) is less common at atmospheric pressure, but is achieved by nanoscale resonators that vibrate mechanically in the microwave range [10].

One key difference between the gas dynamics of atmospheric re-entry and of nanoscale devices is their vastly different Mach numbers,

$$\mathrm{Ma} \equiv \frac{U}{v_{mp}}, \tag{2}$$

where v_{mp} is the most probable gas speed and U is the characteristic bulk flow speed. The gas flow around re-entering vehicles satisfies $\mathrm{Ma} \gg 1$, whereas nanoscale flows exhibit $\mathrm{Ma} \ll 1$. The latter regime and application provides the motivation and focus of this article. Because very small Mach number flows are inherently near thermodynamic equilibrium, the governing Boltzmann equation for these flows can be linearized to simplify analysis.

Theoretical analysis of the Boltzmann equation is complicated by the quadratic nonlinearity and high dimensionality of its collision operator. Bhatnagar, Gross, and Krook [11], and Welander [12] independently proposed the so-called BGK collision model. This model mimics the behavior of a real gas through a single relaxation time process. This eliminates the velocity-space integral of the standard Boltzmann equation which simplifies analytical treatment while retaining important features of the full collision operator [13]. The BGK collision model contains one adjustable parameter, the particle collision frequency, which restricts simultaneous accurate modelling of viscous and thermal effects. Despite this limitation, the BGK model has found great utility in providing insights into rarefied gas flows which have been explored in greater detail using more realistic collision models.

Mathematical complexity of the Boltzmann equation has motivated the development of a multitude of numerical methods. Monte Carlo methods, which simulate the statistical nature of particle-particle collisions and particle-wall collisions, have been developed and applied to steady and unsteady problems [14, 15]. However at low Mach number, which allows linearization of the Boltzmann equation, these Monte Carlo methods can be overwhelmed by statistical noise. A range of methods have consequently been developed that simulate the deviation in the distribution function from equilibrium, alleviating this issue [16–19].

Variational methods involve the construction of a functional whose stationary point is the solution to the Boltzmann equation. This typically utiltizes approximation through the selection of appropriate trial functions. Cercignani [20] developed a general variational approach for the steady linearized Boltzmann equation that is suitable for linearized collision models satisfying general boundary conditions. This was extended by Ladiges & Sader [21] to (unsteady) oscillatory flows. In these variational methods, any error δ in the distribution function propagates as an error δ^2 in the chosen functional. As such, variational methods can yield accurate approximations to physical quantities provided the functional is related to the physical quantity of interest. This principle was applied in Ref. [20] to a variety of gas flow phenomena, including calculation of the velocity slip coefficient to 99% accuracy [22], the mass flow rate for plane Poiseuille flow and the shear flow rate for plane Couette flow. The unsteady extension in Ref. [21] is used in this article to benchmark the derived asymptotic solutions.

Alternate approaches reformulate the Boltzmann equation in terms of bulk macroscopic moments, simplifying analysis. Grad [23] devised a method of expanding the distribution function in multidimensional Hermite polynomials. His thirteen moment method involves the density, three velocity components, the temperature, five independent stress components and three heat flow components—this is achieved through truncation of the distribution function at three terms in a Hermite polynomial expansion. Each moment depends on a higher order moment, so in principle, infinitely many equations are required. Truncating the number of moments in a physically sensible manner, i.e., invoking a closure, is an active area of research [24, 25]. Struchtrup [26, 27] demonstrates that more moments improve agreement with other established methods, while Levermore [24] presents a hierarchy of closures requiring up to 35 moments. As pointed out by Groth [25], the Levermore procedure does not always have a solution for higher order moments. In addition, the number of moment equations is large which can present computational difficulty.

Many asymptotic theories have been developed to solve the Boltzmann equation. The earliest asymptotic model was proposed by Hilbert [28] for a slightly rarefied gas, with matched asymptotic expansions emerging in 1951 [29]. Hilbert considered an isotropic geometric length scale, L, and expanded the distribution function and all its moments with respect to the corresponding Knudsen number. This yielded the required transport equations away from any solid surface in terms of the usual five (continuum) moments of density, bulk velocity and temperature. The required boundary conditions were not formulated until the advent of singular perturbation methods many decades later [30, 31]. Hilbert's name would then become attached to the outer region of these matched asymptotic expansions of the Boltzmann equation [32–36], since he used an identical procedure. Cercignani [30] and Sone [31, 37] considered the steady linearized Boltzmann equation, i.e., $\theta = 0$, imposed a diffusely reflected solid boundary, and derived the appropriate boundary conditions for the Hilbert solution. For example, Cercignani [22, 30] reported a second-order slip model for the tangential bulk velocity, u, for isothermal steady shear flow:

$$u_{\text{wall}} = 1.016k\frac{\partial u}{\partial y}\bigg|_{\text{wall}} - 0.7667k^2\frac{\partial^2 u}{\partial y^2}\bigg|_{\text{wall}}, \tag{3}$$

where $k = (\sqrt{\pi}/2)\text{Kn}$ and y is the normal Cartesian coordinate to the surface; this was later generalised to arbitrary steady/unsteady flows [31, 34, 35, 37]. Equation (3) was investigated by Hadjiconstantinou [38], who demonstrated its accuracy for $\text{Kn} < 0.4$.

Sone's original work for a slightly rarefied gas has been extended to cover nonlinear flows [33] and unsteady linear flows [34–36], all utilizing similar matched asymptotic expansions. In Sone's nonlinear theory [33], an intermediate viscous layer exists near a solid boundary, whose thickness is of order $\sqrt{\text{Kn}}$ smaller than the macroscopic length scale, L. As we shall discuss, this feature parallels the boundary layer structure in this article. For low frequency unsteady linear flows, slip conditions up to $O(\text{Kn}^2)$ were derived in Ref. [35] for the linearized hard sphere and BGK collision operators in the time domain, and in Ref. [34] for the linearized Boltzmann-BGK equation in the frequency domain. These unsteady theories give an incompressible low Reynolds number flow in the Hilbert region. However, viscous diffusion in this region and an implicitly assumed large acoustic wavelength suppress wave phenomena in these theories. Complementary to these studies, Nassios & Sader [36] explored the high frequency (small wavelength) limit.

The Chapman-Enskog expansion, formulated independently by Chapman [39] and Enskog [40], is another method often used to derive the (continuum) Stokes and Navier-Stokes equations from the Boltzmann equation. This approach expands the distribution function in powers of Knudsen number to find successive approximations for the heat flow vector and pressure tensor in terms of the density, velocity, and temperature. At the first three orders in Knudsen number, this leads to the Euler, Navier-Stokes, and Burnett equations, respectively. However, the Burnett and super-Burnett equations possess higher order derivatives without sufficient boundary conditions [34]; closing this system also represents an open research area.

Recently, Aoki *et al.* [41] used a Chapman-Enskog expansion to derive a set of unsteady nonlinear compressible Navier-Stokes-Fourier (NSF) equations. These authors draw on the work of Sone [33] (discussed above) who shows that in the limit of high Reynolds number, a three-layer system forms involving a Knudsen layer of thickness $O(\text{Kn})$, an intermediate viscous (Prandtl) boundary layer of $O(\sqrt{\text{Kn}})$ and an outer inviscid region. By considering the outer two regions, Aoki *et al.* [41] show that the appropriate boundary condition to use with the nonlinear compressible Navier Stokes equation is the Navier slip condition.

Here, we present a formal matched asymptotic analysis of the unsteady linearized Boltzmann-BGK equation, in the limit of small Knudsen number, Kn, and small dimensionless frequency, θ, that accounts for acoustic flows. That is, the acoustic wavelength is comparable to the geometric length scale of the flow. This work utilizes and generalizes the asymptotic frameworks of Refs. [34, 35] where unsteady quasi-incompressible (long wavelength) flows were considered. The reported calculation involves a three-way matched asymptotic expansion with an (outer) Hilbert region, an intermediate viscous boundary layer, and an inner Knudsen boundary layer. This leads to a system of transport equations and boundary condition correct to $O(\text{Kn})$. Interestingly, we find that the slip boundary condition appears at $O(\sqrt{\text{Kn}})$, in contrast to previous studies that assume long wavelength [34, 35].

The purpose of this article is to detail the (frequency-domain) asymptotic theory reported in the Masters thesis (2018) of the first author and complete the analysis of its applications [42]: (1) one-dimensional flow generated between two planar walls, (2) two-dimensional thermal creep between two walls, and (3) three-dimensional axisymmetric flow generated by an oscillating sphere. We also provide a comparison to previous asymptotic analyses and direct numerical solutions of the Boltzmann-BGK equation. Together, the study of these applications provides a comprehensive validation of the asymptotic theory across a range of spatial dimensionalities. We recently became aware of independent work by Takata & Hattori [43] that reports the complementary time-domain formulation—which is related to the present frequency-domain formulation by the ansatz in Eq. (12)—where the single application of one-dimensional wave generation by an oscillating plane wall was studied (with several collision models). Formulation in the frequency-domain is natural due to the foundational use of the linearized Boltzmann equation, employed in both studies. The present work thus provides a significant advance in the applications studied, which robustly demonstrates the validity of the asymptotic theory and its utility across a broad array of problems. Importantly, use of a time-domain formulation can generate secular terms that grow in both time and space [43], i.e., when operating on resonance. In the present frequency-domain formulation, this time-based secularity appears naturally as frequency-based singularities. Ref. [43] presents a remedy to this issue via a modification of the compressible Navier-Stokes-Fourier system of Aoki [41] that retains the $O(\epsilon^2)$ accuracy of the theory. The same regularization can be used in the frequency-domain. Here, we demonstrate and discuss the features/limitations of the (simpler) compressible Navier-Stokes-Fourier system of Aoki [41] via the applications studied; this constitutes a standard implementation of conventional hydrodynamics with a Navier slip condition.

This article is presented in four sections. The problem formulation and its solution method are outlined in Section II. This is followed by a discussion of the boundary layer structure and derivation of the transport equations in all regions. Section III discusses the transport equations and reports the slip conditions. A comparison to existing results is also made. Finally, the developed theory is applied to the three model applications and a comparison to independent results is reported.

II. PROBLEM FORMULATION

We consider a general flow of a gas obeying the BGK collision model near a solid boundary or boundaries. This flow is to be solved subject to the assumptions used in previous asymptotic analyses of the Boltzmann equation: Solid boundaries move sinusoidally in time with angular frequency, ω; net mass flux at the solid boundaries is zero; the gas flow is in the small Mach number and small Knudsen number regimes; the solid boundaries reflect incoming gas particles diffusely. The difference here is that the the resulting acoustic wavelength is comparable to the macroscopic length scale, allowing for the modelling of acoustic effects.

The mass distribution function, F, satisfies the BGK equation [11, 12, 44],

$$\frac{\partial F}{\partial t} + v_i \frac{\partial F}{\partial x_i} + a_i \frac{\partial F}{\partial v_i} = \nu(\rho(\boldsymbol{x}, t) f_0(\boldsymbol{x}, \boldsymbol{v}, t) - F), \tag{4}$$

where a_i is the external body force per unit mass [45], x_i and v_i are the position and gas particle velocity, respectively, ν is the collision frequency, and $\rho(\boldsymbol{x}, t)$ is the local (bulk) gas density. The local (equilibrium) Maxwell-Boltzmann velocity distribution is given by

$$f_0(\boldsymbol{x}, \boldsymbol{v}, t) = \left(\frac{1}{\sqrt{\pi} v_{mp}(T)}\right)^3 \exp\left(-\left(\frac{v_i - \bar{v}_i}{v_{mp}(T)}\right)^2\right), \tag{5}$$

where $\bar{v}_i(\boldsymbol{x}, t)$ is the local mean gas velocity and $v_{mp}(T)$ is the most probable gas velocity at the local temperature $T(\boldsymbol{x}, t)$,

$$v_{mp}(T) = \sqrt{\frac{2 k_B T}{m}}, \tag{6}$$

where k_B is the Boltzmann constant. The local (bulk) density ρ, velocity $\bar{v}_i$, temperature T, pressure p, pressure tensor p_{ij}, and heat flow vector q_i are given by the following moments,

$$\rho = \int_{\mathbb{R}^3} F\, d^3\boldsymbol{v}, \tag{7a}$$

$$\bar{v}_i = \frac{1}{\rho}\int_{\mathbb{R}^3} v_i F\, d^3\boldsymbol{v}, \tag{7b}$$

$$\frac{3k_BT}{m} = \frac{1}{\rho}\int_{\mathbb{R}^3} (v_i - \bar{v}_i)^2 F\, d^3\boldsymbol{v}, \tag{7c}$$

$$p = \frac{\rho k_B T}{m}, \tag{7d}$$

$$p_{ij} = \int_{\mathbb{R}^3} (v_i - \bar{v}_i)(v_j - \bar{v}_j) F\, d^3\boldsymbol{v}, \tag{7e}$$

$$q_i = \frac{1}{2}\int_{\mathbb{R}^3} (v_i - \bar{v}_i)(v_j - \bar{v}_j)^2 F\, d^3\boldsymbol{v}, \tag{7f}$$

where the equation of state for a dilute gas is the ideal gas law in Eq. (7d), and $d^3\boldsymbol{v}$ is the usual volume element for three-dimensional velocity space. Mass, momentum, and energy are conserved over intermolecular collisions [44],

$$\int_{\mathbb{R}^3} (\rho(\boldsymbol{x},t) f_0(\boldsymbol{x},\boldsymbol{v},t) - F)\, \Phi\, d^3\boldsymbol{v} = 0, \tag{8}$$

where $\Phi = 1, v_j, v_j^2$, respectively.

Because we study small Mach number flows, i.e., $\mathrm{Ma} \ll 1$, the distribution function, F, is expressed as

$$F = \rho_0 E_0 (1 + \mathrm{Ma}\, \phi(\boldsymbol{x},\boldsymbol{v},t)), \tag{9}$$

and linearized with respect to Ma. Henceforth, all symbols with subscript 0 are at equilibrium, and

$$E_0 = \left(\frac{1}{\sqrt{\pi} v_{mp}(T_0)}\right)^3 \exp\left(-\left(\frac{v_i}{v_{mp}(T_0)}\right)^2\right). \tag{10}$$

Similarly, the scaled linearized transport variables are given by

$$\begin{gathered} \rho = \rho_0(1 + \mathrm{Ma}\,\sigma(\boldsymbol{x},t)), \qquad \bar{v}_i = \mathrm{Ma}\,\bar{v}_i', \qquad T = T_0(1 + \mathrm{Ma}\,\tau(\boldsymbol{x},t)), \\ p = p_0(1 + \mathrm{Ma}\,P(\boldsymbol{x},t)), \qquad p_{ij} = p_0(\delta_{ij} + \mathrm{Ma}\,P_{ij}(\boldsymbol{x},t)), \qquad q_i = \mathrm{Ma}\,p_0 v_{mp}(T_0)\hat{q}_i. \end{gathered} \tag{11}$$

For brevity, we shall refer to ϕ simply as the distribution function, rather than the distribution function perturbation, and similarly for its macroscopic transport variables. All time-varying functions (denoted α) are expressed as

$$\alpha(\boldsymbol{x},\boldsymbol{v},t) = \tilde{\alpha}(\boldsymbol{x},\boldsymbol{v}) e^{-i\omega t}. \tag{12}$$

For simplicity, we omit the '$\sim$' notation and note that henceforth all dependent functions are frequency-dependent expressions. The prime symbol in $\bar{v}_i'$ is also omitted from this point forward for simplicity.

Linearizing the Boltzmann-BGK equation gives [34]

$$-i\omega\phi + v_i\frac{\partial\phi}{\partial x_i} - \frac{2v_i a_i}{v_{mp}(T_0)^2} = \nu\left(\sigma + \frac{2v_i}{v_{mp}(T_0)}\bar{v}_i + \left(\frac{v_j^2}{v_{mp}(T_0)^2} - \frac{3}{2}\right)\tau - \phi\right). \tag{13}$$

Gas particles reflect diffusely from the solid boundary which is moved with velocity, $\mathrm{Ma}\,V_i$,. In the low Mach number limit, as particle speeds greatly exceed the solid boundary velocities, the boundary condition in Eq. (2.17) of [34] can be simplified to Eq. (14).

$$\phi_b = \sigma_b + \frac{2v_i}{v_{mp}(T_0)^2}V_i + \left(\frac{v_i^2}{v_{mp}(T_0)^2} - \frac{3}{2}\right)\tau_b, \qquad v_i n_i > 0. \tag{14}$$

Zero net mass flux at the solid boundary leads to the corresponding linear relation [34],

$$\sigma_b = -\frac{1}{2}\tau_b + \sqrt{\pi}\frac{V_i n_i}{v_{mp}(T_0)} - 2\sqrt{\pi}\int_{v_i n_i \le 0} \frac{v_j n_j}{v_{mp}(T_0)}\phi E(\boldsymbol{v}) d^3\boldsymbol{v}. \tag{15}$$

The no-penetration condition is

$$\bar{v}_i n_i = V_i n_i. \tag{16}$$

It can be shown that Eq. (15) is implicit in the no-penetration and diffuse boundary condition, so it will not be used explicitly.

A. Three-layer structure of the acoustic flow

Acoustic phenomena occur when the flow wavelength,

$$\Lambda \equiv \frac{v_{mp}}{\omega}, \tag{17}$$

is comparable to the macroscopic length scale, L, of the flow. This can be expressed in terms of the acoustic wave number,

$$\zeta \equiv \frac{L}{\Lambda} = \frac{1}{2}\beta k, \tag{18}$$

where $k = (\sqrt{\pi}/2)\mathrm{Kn}$ is the reduced Knudsen number, and the Stokes parameter is

$$\beta \equiv \left(\frac{L}{\delta}\right)^2 = \frac{\omega L^2}{\nu_{\mathrm{kin}}}. \tag{19}$$

Here, $\nu_{\mathrm{kin}} = (\sqrt{\pi}/4)v_{mp}\lambda$ is the gas kinematic viscosity [32, 34] and δ is the usual viscous penetration depth. For wave effects to occur, we require the acoustic wavenumber, ζ, to be $O(1)$. It then follows from Eq. (18) that $\beta = O\left(1/k\right)$, or equivalently,

$$\frac{\delta}{L} = O\left(\sqrt{k}\right). \tag{20}$$

This shows that the viscous penetration depth is dictated by the gas mean free path—it is not an independent parameter as in previous studies [34, 35] that focused on long wavelength (quasi-incompressible) flows. Therefore, a three-layer structure exists in these acoustic flows where the thickness of each boundary layer separately vanishes asymptotically in the limit of small k, i.e., a slightly rarefied gas. Figure 1 shows this three-layer structure along with previous studies that considered slightly rarefied flows ($k \ll 1$). (i) long wavelength (quasi-incompressible), $\Lambda = O(L/k)$, and low frequency, $\omega \ll \nu$, which leads to the usual two-layer structure [34, 35]; and (ii) short wavelength, $\Lambda \ll \lambda \ll L$, and high frequency, $\omega \gg \nu$, that produces a different three-layer structure [36].

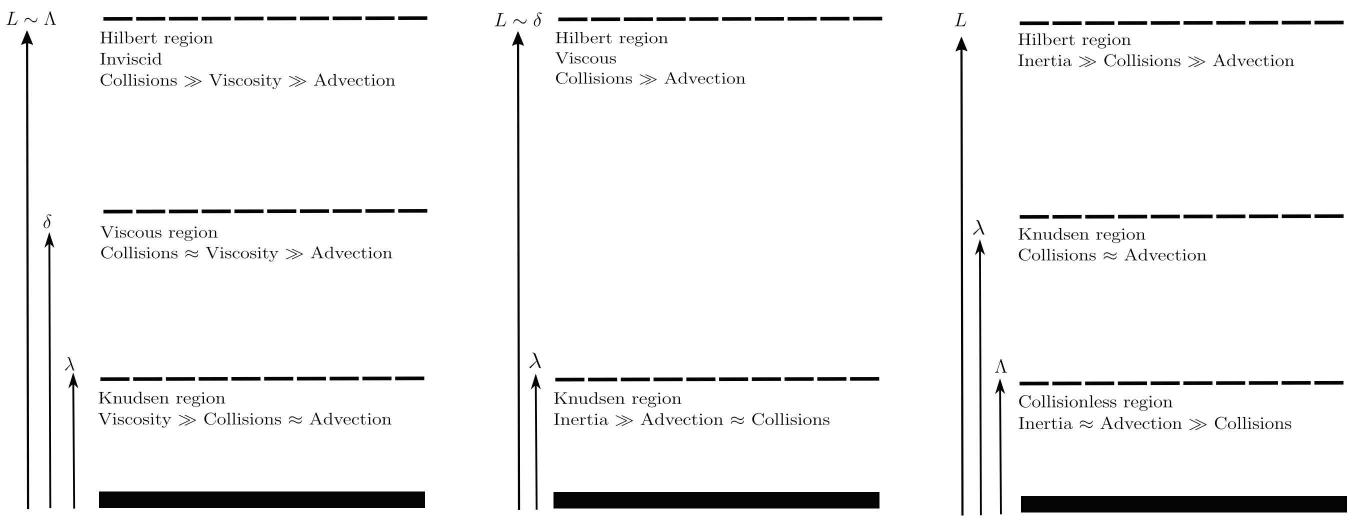

FIG. 1: Boundary layer structures for slightly rarefied flows. Left panel: Present study of acoustic flows with $\zeta = O(1)$, showing the three-layer structure with the thickness of each layer separated by a multiplicative factor of $\sqrt{k}$. Middle panel: Quasi-incompressible (long wavelength) flows with $\zeta \ll 1$ [34, 35]. Right panel: High frequency flows with $\zeta \gg 1/k \gg 1$ [36].

It is easy to show that

$$\frac{\omega}{\nu} = \zeta k, \tag{21}$$

which establishes that the present acoustic problem also coincides with the low frequency limit, $\omega \ll \nu$, because $\zeta = O(1)$.

The presence of the length scale, $\sqrt{k}$, in the current acoustic problem motivates an asymptotic expansion in the small parameter, $\sqrt{k}$, rather than the usual k. This three-layered system also features in Sone's general nonlinear theory for steady but finite Mach number flow [33]. Indeed, our analysis has many similarities with Sone's formulation, yet it applies to the opposite limit of low Mach number unsteady flow. Takata *et al.* [35] hint at the existence of such a three-layered system on a suitable frequency scale.

III. MATCHED ASYMPTOTIC EXPANSION

We now provide details of the matched asymptotic expansion used to solve the flow problem in the limit of small scaled Knudsen number, k. From this point forward, all particle velocities refer to their non-dimensional quantities, scaled by $v_{mp}(T_0)$, while bulk velocities are scaled by $U \equiv \mathrm{Ma}\, v_{mp}(T_0)$; see Eq. (2).

A. Hilbert region

In the furthest region from the solid surface, the Hilbert region (see Fig. 1a), the flow problem is non-dimensionlized using the isotropic and macroscopic length scale, L. The linearized scaled Boltzmann equation, Eq. (13), becomes

$$-i\zeta\phi_H + v_i \frac{\partial \phi_H}{\partial x_i} - 2\zeta v_i a_i = \frac{1}{k}\left(Q_H - \phi_H\right), \tag{22}$$

with the linearized equilibrium,

$$Q_A = \sigma_A + 2\bar{v}_{A|i} v_i + \left(v_i^2 - \frac{3}{2}\right)\tau_A, \tag{23}$$

where A is either H, V or K which respectively refer to the Hilbert, viscous and Knudsen regions.

Following the analysis in Section II A, we define $\epsilon \equiv \sqrt{k}$ and expand the distribution function, ϕ_H, its moments, the Boltzmann equation (Eq. (22)), in powers of ϵ,

$$\alpha = \sum_{n=0}^{\infty} \epsilon^n \alpha^{(n)}, \tag{24}$$

where α represents any of these dependent functions, and $\alpha^{(n)}$ is the n^{th} component. Substituting Eq. (24) into Eq. (22) gives

$$0 = Q_H^{(0)} - \phi_H^{(0)}, \tag{25a}$$
$$0 = Q_H^{(1)} - \phi_H^{(1)}, \tag{25b}$$
$$-i\zeta\phi_H^{(0)} + v_i \frac{\partial \phi_H^{(0)}}{\partial x_i} - 2\zeta v_i a_i = Q_H^{(2)} - \phi_H^{(2)}, \tag{25c}$$
$$-i\zeta\phi_H^{(n-2)} + v_i \frac{\partial \phi_H^{(n-2)}}{\partial x_i} = Q_H^{(n)} - \phi_H^{(n)}, \quad n \geq 3. \tag{25d}$$

The collision invariants (see Eq. (8)) hold in all regions and can be linearized to give

$$\int_{\mathbb{R}^3} (Q_A^{(n)} - \phi_A^{(n)})\Phi \, d^3\boldsymbol{v} = 0, \tag{26}$$

where A is defined in Eq. (23). These solvability conditions, when applied to the Hilbert equations, Eq. (25), yield the system of governing equations in Table I. The issue of closure of these governing equations is deferred to Section III G.

$n = 0$

$$i\zeta\sigma_H^{(0)} = \frac{\partial \bar{v}_{H|i}^{(0)}}{\partial x_i},$$
$$i\zeta\bar{v}_{H|j}^{(0)} + \zeta a_j = \frac{1}{2}\frac{\partial P_H^{(0)}}{\partial x_j},$$
$$\tau_H^{(0)} = \frac{2}{3}\sigma_H^{(0)},$$
$$P_{H|ij}^{(0)} = P_H^{(0)}\delta_{ij},$$
$$q_{H|i}^{(0)} = 0,$$

$n = 1$

$$i\zeta\sigma_H^{(1)} = \frac{\partial \bar{v}_{H|i}^{(1)}}{\partial x_i},$$
$$i\zeta\bar{v}_{H|j}^{(1)} = \frac{1}{2}\frac{\partial P_H^{(1)}}{\partial x_j},$$
$$\tau_H^{(1)} = \frac{2}{3}\sigma_H^{(1)},$$
$$P_{H|ij}^{(1)} = P_H^{(1)}\delta_{ij},$$
$$q_{H|i}^{(1)} = 0,$$

$n = 2$

$$i\zeta\sigma_H^{(2)} = \frac{\partial \bar{v}_{H|i}^{(2)}}{\partial x_i},$$
$$i\zeta\bar{v}_{H|j}^{(2)} = \frac{1}{2}\frac{\partial P_H^{(2)}}{\partial x_j} - \frac{1}{2}\left(\frac{1}{3}\frac{\partial}{\partial x_j}\left(\frac{\partial \bar{v}_{H|w}^{(0)}}{\partial x_w}\right) + \frac{\partial^2 \bar{v}_{H|j}^{(0)}}{\partial {x_k}^2}\right),$$
$$i\zeta\tau_H^{(2)} = \frac{2}{3}i\zeta\sigma_H^{(2)} - \frac{5}{6}\frac{\partial^2 \tau_H^{(0)}}{\partial {x_i}^2},$$
$$P_{H|ij}^{(2)} = \left(P_H^{(2)} + i\zeta\tau_H^{(0)}\right)\delta_{ij} - \left(\frac{\partial \bar{v}_{H|j}^{(0)}}{\partial x_i} + \frac{\partial \bar{v}_{H|k}^{(0)}}{\partial x_j}\right),$$
$$q_{H|i}^{(2)} = -\frac{5}{4}\frac{\partial \tau_H^{(0)}}{\partial x_i}.$$

TABLE I: Bulk transport equations in Hilbert region up to second order in ϵ.

B. Viscous boundary layer

Flow in the intermediate region, termed the 'viscous boundary layer' (see Fig. 1a), varies rapidly in the direction normal to the solid surface with a length scale $\delta \equiv \epsilon L$. As per Ref. [33], the surface geometry within this viscous region is specified using the method of moving frame, where a local orthonormal coordinate system is introduced comprising two (principal) tangent vectors, t_i^1 and t_i^2, and an associated outward wall-normal, n_i. The new orthogonal curvilinear coordinate system is

$$x_i \equiv \epsilon y n_i(\chi_1, \chi_2) + x_{wi}(\chi_1, \chi_2), \tag{27}$$

where y is the non-dimensionlized Cartesian coordinate normal to the solid surface (scaled by δ) increasing away from the wall, n_i is the surface outward normal and x_{wi} is the corresponding tangential Cartesian coordinate (scaled by L), with

$$\left(\frac{\partial \chi_j}{\partial x_i}\right)_0 || \, t_i^j, \qquad t_k^p t_k^q = \delta_{pq}, \tag{28}$$

where $p, q = 1, 2$, the subscript 0 denotes the value at $y = 0$ and (n_i, t_i^1, t_i^2) forms a right-handed coordinate system. Note that the indices j, p, q, are not tensorial.

The non-dimensional linearized Boltzmann equation in this region (denoted using the subscript V) is

$$-i\zeta\epsilon^2\phi_V + \epsilon v_i n_i \frac{\partial \phi_V}{\partial y} + \epsilon^2 v_i \left(\frac{\partial \chi_1}{\partial x_i}\frac{\partial \phi_V}{\partial \chi_1} + \frac{\partial \chi_2}{\partial x_i}\frac{\partial \phi_V}{\partial \chi_2} \right) - 2\epsilon^2 \zeta v_i a_i = Q_V - \phi_V . \tag{29}$$

The coordinate gradients $\frac{\partial \chi_1}{\partial x_i}, \frac{\partial \chi_2}{\partial x_i}$ may depend on the rescaled normal coordinate, y, in the viscous region (length scale is ϵ).

The curvature terms, which define contributions from the surface shape, are expanded in a power series in $r \equiv (x_i - x_{wi})n_i$, assuming a sufficiently smooth boundary:

$$\frac{\partial \chi_1}{\partial x_i} = \left(\frac{\partial \chi_1}{\partial x_i}\right)_0 + \epsilon y \left(\frac{\partial}{\partial r}\left(\frac{\partial \chi_1}{\partial x_i}\right)\right)_0 + \frac{1}{2}\epsilon^2 y^2 \left(\frac{\partial^2}{\partial r^2}\left(\frac{\partial \chi_1}{\partial x_i}\right)\right)_0 \cdots , \tag{30}$$

and similarly for χ_2, where the subscript 0 indicate evaluation at the surface, $y = 0$.

The viscous distribution function and associated bulk moments are expanded accordingly,

$$\phi_V = \sum_{n=0}^{\infty} \epsilon^n \phi_V^{(n)} . \tag{31}$$

The corresponding Boltzmann equation in this viscous region, at each order in ϵ, is

$$0 = Q_V^{(0)} - \phi_V^{(0)}, \tag{32a}$$

$$v_i n_i \frac{\partial \phi_V^{(0)}}{\partial y} = Q_V^{(1)} - \phi_V^{(1)}, \tag{32b}$$

$$\begin{aligned} -i\zeta\phi_V^{(0)} + v_i n_i \frac{\partial \phi_V^{(1)}}{\partial y} + v_i \left(\left(\frac{\partial \chi_1}{\partial x_i}\right)_0 \frac{\partial \phi_V^{(0)}}{\partial \chi_1} + \left(\frac{\partial \chi_2}{\partial x_i}\right)_0 \frac{\partial \phi_V^{(0)}}{\partial \chi_2} \right) \\ -2\zeta v_i a_{i,0} = Q_V^{(2)} - \phi_V^{(2)}, \end{aligned} \tag{32c}$$

$$\begin{aligned} -i\zeta\phi_V^{(1)} + v_i n_i \frac{\partial \phi_V^{(2)}}{\partial y} + v_i \left(\left(\frac{\partial \chi_1}{\partial x_i}\right)_0 \frac{\partial \phi_V^{(1)}}{\partial \chi_1} + \left(\frac{\partial \chi_2}{\partial x_i}\right)_0 \frac{\partial \phi_V^{(1)}}{\partial \chi_2} \right) \\ + y v_i \left(\left(\frac{\partial}{\partial r}\left(\frac{\partial \chi_1}{\partial x_i}\right)\right)_0 \frac{\partial \phi_V^{(0)}}{\partial \chi_1} + \left(\frac{\partial}{\partial r}\left(\frac{\partial \chi_2}{\partial x_i}\right)\right)_0 \frac{\partial \phi_V^{(0)}}{\partial \chi_2} \right) \\ -2\zeta v_i \left(\frac{\partial a_i}{\partial r}\right)_0 = Q_V^{(3)} - \phi_V^{(3)}, \end{aligned} \tag{32d}$$

$$\begin{aligned} -i\zeta\phi_V^{(2)} + v_i n_i \frac{\partial \phi_V^{(3)}}{\partial y} + v_i \left(\left(\frac{\partial \chi_1}{\partial x_i}\right)_0 \frac{\partial \phi_V^{(2)}}{\partial \chi_1} + \left(\frac{\partial \chi_2}{\partial x_i}\right)_0 \frac{\partial \phi_V^{(2)}}{\partial \chi_2} \right) \\ + y v_i \left(\left(\frac{\partial}{\partial r}\left(\frac{\partial \chi_1}{\partial x_i}\right)\right)_0 \frac{\partial \phi_V^{(1)}}{\partial \chi_1} + \left(\frac{\partial}{\partial r}\left(\frac{\partial \chi_2}{\partial x_i}\right)\right)_0 \frac{\partial \phi_V^{(1)}}{\partial \chi_2} \right) \\ + \frac{1}{2} y^2 v_i \left(\left(\frac{\partial^2}{\partial r^2}\left(\frac{\partial \chi_1}{\partial x_i}\right)\right)_0 \frac{\partial \phi_V^{(0)}}{\partial \chi_1} + \left(\frac{\partial^2}{\partial r^2}\left(\frac{\partial \chi_2}{\partial x_i}\right)\right)_0 \frac{\partial \phi_V^{(0)}}{\partial \chi_2} \right) \\ -2\zeta v_i \left(\frac{\partial^2 a_i}{\partial r^2}\right)_0 = Q_V^{(4)} - \phi_V^{(4)}, \end{aligned} \tag{32e}$$

where $\phi_V^{(0)}$ is the Maxwellian defined in Eq. (23).

The transport equations in the viscous region are derived using the collision invariants, Eq. (26), and are given in Table II. Corresponding equations in the t_i^2 direction are obtained by interchanging t_i^1 with t_i^2 and χ_1 with χ_2. As with the Hilbert equations, closure of this system is discussed in Section III G.

The set of equations in Table II are expressed in terms of curvature coefficients in Appendix C [32, 34, 46].

$n = 0$

$$\frac{\partial P_V^{(0)}}{\partial y} = 0,$$

$$\frac{\partial \bar{v}_{V|i}^{(0)} n_i}{\partial y} = 0,$$

$$\frac{\partial^2 \bar{v}_{V|i}^{(0)} t_i^1}{\partial y^2} + 2i\zeta \bar{v}_{V|i}^{(0)} t_i^1 = t_i^1 \left(\frac{\partial \chi_1}{\partial x_i}\right)_0 \frac{\partial P_V^{(0)}}{\partial \chi_1} - 2\zeta a_{i,0} t_i^1,$$

$$\frac{\partial^2 \tau_V^{(0)}}{\partial y^2} + 2i\zeta \tau_V^{(0)} = \tfrac{4}{5} i\zeta P_V^{(0)},$$

$$P_{V|ij}^{(0)} = P_V^{(0)} \delta_{ij},$$

$$q_{V|i}^{(0)} = 0,$$

$n = 1$

$$\frac{\partial P_V^{(1)}}{\partial y} = 2i\zeta \bar{v}_{V|i}^{(0)} n_i + 2\zeta a_{i,0} n_i,$$

$$\frac{\partial \bar{v}_{V|i}^{(1)} n_i}{\partial y} = i\zeta \sigma_V^{(0)} - \left(\left(\frac{\partial \chi_1}{\partial x_i}\right)_0 \frac{\partial}{\partial \chi_1} + \left(\frac{\partial \chi_2}{\partial x_i}\right)_0 \frac{\partial}{\partial \chi_2}\right) v_{V|i}^{(0)},$$

$$\frac{\partial^2 \bar{v}_{V|i}^{(1)} t_i^1}{\partial y^2} + 2i\zeta \bar{v}_{V|i}^{(1)} t_i^1 = t_i^1 \left(\left(\frac{\partial \chi_1}{\partial x_j}\right)_0 \frac{\partial}{\partial \chi_1} + \left(\frac{\partial \chi_2}{\partial x_j}\right)_0 \frac{\partial}{\partial \chi_2}\right)\left(P_V^{(1)} \delta_{ij} - \frac{\partial}{\partial y}\left(\bar{v}_{V|j}^{(0)} n_i + \bar{v}_{V|i}^{(0)} n_j\right)\right) -$$
$$\frac{\partial}{\partial y}\left(n_j t_i^1 \left(\left(\frac{\partial \chi_1}{\partial x_i}\right)_0 \frac{\partial \bar{v}_{V|j}^{(0)}}{\chi_1}\right)\right) + y t_i^1 \left(\frac{\partial}{\partial r}\left(\left(\frac{\partial \chi_1}{\partial x_i}\right)_0\right) \frac{\partial P_V^{(0)}}{\partial \chi_1}\right) - 2y t_i^1 \zeta \left(\frac{\partial a_i}{\partial r}\right)_0,$$

$$\frac{\partial^2 \tau_V^{(1)}}{\partial y^2} + 2i\zeta \tau_V^{(1)} = \tfrac{4}{5} i\zeta P_V^{(1)} + \left(\left(\frac{\partial \chi_1}{\partial x_j}\right)_0 \frac{\partial}{\partial \chi_1} + \left(\frac{\partial \chi_2}{\partial x_j}\right)_0 \frac{\partial}{\partial \chi_2}\right)\left(\frac{\partial \sigma_V^{(0)}}{\partial y} n_j\right),$$

$$P_{V|ij}^{(1)} = P_V^{(1)} \delta_{ij} - \frac{\partial}{\partial y}\left(\bar{v}_{V|i}^{(0)} n_j + \bar{v}_{V|j}^{(0)} n_i\right),$$

$$q_{V|i}^{(1)} = -\tfrac{5}{4} \frac{\partial \tau_V^{(0)}}{\partial y} n_i,$$

$n = 2$

$$\frac{\partial \bar{v}_{V|i}^{(2)} n_i}{\partial y} = i\zeta \sigma_V^{(1)} - \left(\left(\frac{\partial \chi_1}{\partial x_j}\right)_0 \frac{\partial}{\partial \chi_1} + \left(\frac{\partial \chi_2}{\partial x_j}\right)_0 \frac{\partial}{\partial \chi_2}\right) \bar{v}_{V|j}^{(1)} - y\left(\left(\frac{\partial}{\partial r}\left(\frac{\partial \chi_1}{\partial x_j}\right)\right)_0 \frac{\partial}{\partial \chi_1} + \left(\frac{\partial}{\partial r}\left(\frac{\partial \chi_2}{\partial x_j}\right)\right)_0 \frac{\partial}{\partial \chi_2}\right) \bar{v}_{V|j}^{(0)},$$

$$\frac{\partial P_V^{(2)}}{\partial y} = 2i\zeta \bar{v}_{V|i}^{(1)} n_i + 2y n_i \zeta \left(\frac{\partial a_i}{\partial r}\right)_0 - \frac{\partial}{\partial y}\left(\left(\frac{\partial \chi_1}{\partial x_j}\right)_0 \frac{\partial}{\partial \chi_1} + \left(\frac{\partial \chi_2}{\partial x_j}\right)_0 \frac{\partial}{\partial \chi_2}\right)\left(\bar{v}_{V|j}^{(1)}\right),$$

$$\frac{\partial^2 \bar{v}_{V|i}^{(2)} t_i^1}{\partial y^2} + 2i\zeta \bar{v}_{V|i}^{(2)} t_i^1 = -\tfrac{3}{2} \frac{\partial^4 \bar{v}_{V|i}^{(0)} t_i^1}{\partial y^4} - \frac{\partial}{\partial y}\left(n_j t_i^1 \left(\frac{\partial \chi_1}{\partial x_i}\right)_0 \frac{\partial \bar{v}_{V|j}^{(1)}}{\partial \chi_1}\right) +$$
$$t_i^1 \left(\left(\frac{\partial \chi_1}{\partial x_j}\right)_0 \frac{\partial}{\partial \chi_1} + \left(\frac{\partial \chi_2}{\partial x_j}\right)_0 \frac{\partial}{\partial \chi_2}\right)\left(\delta_{ij} P_V^{(2)} + i\zeta \tau_V^{(0)} \delta_{ij} - \left(\frac{\partial}{\partial y}\left(\bar{v}_{V|j}^{(1)} n_i + \bar{v}_{V|i}^{(1)} n_j\right)\right)\right) -$$
$$t_i^1 \left(\left(\frac{\partial \chi_1}{\partial x_j}\right)_0 \frac{\partial}{\partial \chi_1} + \left(\frac{\partial \chi_2}{\partial x_j}\right)_0 \frac{\partial}{\partial \chi_2}\right)\left(\left(\frac{\partial \chi_1}{\partial x_k}\right)_0 \frac{\partial}{\partial \chi_1} + \left(\frac{\partial \chi_2}{\partial x_k}\right)_0 \frac{\partial}{\partial \chi_2}\right)\left(\bar{v}_{V|j}^{(0)} \delta_{ik} + \bar{v}_{V|i}^{(0)} \delta_{jk}\right) + \tfrac{3}{2} \frac{\partial^2}{\partial y^2}\left(t_i^1 \left(\frac{\partial \chi_1}{\partial x_i}\right)_0 \frac{\partial \tau_V^{(0)}}{\partial \chi_1}\right) -$$
$$2i\zeta \frac{\partial^2 \bar{v}_{V|i}^{(0)} t_i^1}{\partial y^2} - \frac{\partial}{\partial y}\left(y n_j t_i^1 \left(\frac{\partial}{\partial r}\left(\frac{\partial \chi_1}{\partial x_i}\right)\right)_0 \frac{\partial \bar{v}_{V|j}^{(0)}}{\partial \chi_1}\right) +$$
$$t_i^1 y \left(\left(\frac{\partial}{\partial r}\left(\frac{\partial \chi_1}{\partial x_j}\right)\right)_0 \frac{\partial}{\partial \chi_1} + \left(\frac{\partial}{\partial r}\left(\frac{\partial \chi_2}{\partial x_j}\right)\right)_0 \frac{\partial}{\partial \chi_2}\right)\left(P_V^{(1)} \delta_{ij} - \frac{\partial}{\partial y}\left(\bar{v}_{V|i}^{(0)} n_j + \bar{v}_{V|j}^{(0)} n_i\right)\right) + \tfrac{1}{2} y^2 \left(t_i^1 \left(\frac{\partial^2}{\partial r^2}\left(\frac{\partial \chi_1}{\partial x_i}\right)\right)_0 \frac{\partial P_V^{(0)}}{\partial \chi_1}\right) -$$
$$y^2 t_i^1 \zeta \left(\frac{\partial^2 a_i}{\partial r^2}\right)_0,$$

$$\frac{\partial^2 \tau_V^{(2)}}{\partial y^2} + 2i\zeta \tau_V^{(2)} = \tfrac{4}{5} i\zeta P_V^{(2)} + \tfrac{11}{5} i\zeta \frac{\partial^2 \tau_V^{(0)}}{\partial y^2} + \frac{\partial^2}{\partial y^2}\left(\left(\frac{\partial \chi_1}{\partial x_k}\right)_0 \frac{\partial}{\partial \chi_1} + \left(\frac{\partial \chi_2}{\partial x_k}\right)_0 \frac{\partial}{\partial \chi_2}\right)\left(\bar{v}_{V|k}^{(0)}\right) +$$
$$\left(\left(\frac{\partial \chi_1}{\partial x_j}\right)_0 \frac{\partial}{\partial \chi_1} + \left(\frac{\partial \chi_2}{\partial x_j}\right)_0 \frac{\partial}{\partial \chi_2}\right)\left(2i\zeta \bar{v}_{V|j}^{(0)} - 2\zeta a_{j,0} - n_j \frac{\partial}{\partial y}(\sigma_V^{(1)} + 2\tau_V^{(1)}) - n_j \left(\frac{\partial a_j}{\partial r}\right)_0\right) -$$
$$\left(\left(\frac{\partial \chi_1}{\partial x_j}\right)_0 \frac{\partial}{\partial \chi_1} + \left(\frac{\partial \chi_2}{\partial x_j}\right)_0 \frac{\partial}{\partial \chi_2}\right)^2 \left(\sigma_V^{(0)} + 2\tau_V^{(0)}\right) + y\left(\left(\frac{\partial}{\partial r}\left(\frac{\partial \chi_1}{\partial x_j}\right)\right)_0 \frac{\partial}{\partial \chi_1} + \left(\frac{\partial}{\partial r}\left(\frac{\partial \chi_2}{\partial x_j}\right)\right)_0 \frac{\partial}{\partial \chi_2}\right)\left(\frac{\partial \sigma_V^{(0)}}{\partial y} n_j\right),$$

$$P_{V|ij}^{(2)} = \delta_{ij}\left(P_V^{(2)} + \tfrac{2}{5} i\zeta P_V^{(0)}\right) - \frac{\partial}{\partial y}\left(\bar{v}_{V|i}^{(1)} n_j + \bar{v}_{V|j}^{(1)} n_i\right) + \frac{\partial^2 \tau_V^{(0)}}{\partial y^2} n_i n_j - \left(\left(\frac{\partial \chi_1}{\partial x_i}\right)_0 \frac{\partial}{\partial \chi_1} - \left(\frac{\partial \chi_2}{\partial x_i}\right)_0 \frac{\partial}{\partial \chi_2}\right) \bar{v}_{V|j}^{(0)},$$
$$-\left(\left(\frac{\partial \chi_1}{\partial x_j}\right)_0 \frac{\partial}{\partial \chi_1} + \left(\frac{\partial \chi_2}{\partial x_j}\right)_0 \frac{\partial}{\partial \chi_2}\right) \bar{v}_{V|i}^{(0)},$$

$$q_{V|i}^{(2)} = -\tfrac{5}{4} \frac{\partial \tau_V^{(1)}}{\partial y} n_i + \tfrac{1}{2} \frac{\partial^2 \bar{v}_{V|i}^{(0)}}{\partial y^2} - \tfrac{5}{4}\left(\left(\frac{\partial \chi_1}{\partial x_i}\right)_0 \frac{\partial}{\partial \chi_1} + \left(\frac{\partial \chi_2}{\partial x_i}\right)_0 \frac{\partial}{\partial \chi_2}\right) \tau_V^{(0)}.$$

TABLE II: Transport equations in the viscous region.

C. Knudsen layer

The scaled coordinates in the Knudsen region are

$$x_i = \epsilon^2 \eta n_i(\chi_1, \chi_2) + x_{wi}(\chi_1, \chi_2). \tag{33}$$

The solution in this region is expressed as the sum of the viscous solution, ϕ_V, and a Knudsen correction, ϕ_K, whose governing equation is

$$-i\zeta\epsilon^2\phi_K + v_i n_i \frac{\partial \phi_K}{\partial \eta} + \epsilon^2 v_i \left(\frac{\partial \chi_1}{\partial x_i}\frac{\partial}{\partial \chi_1} + \frac{\partial \chi_2}{\partial x_i}\frac{\partial}{\partial \chi_2} \right) \phi_K = Q_K - \phi_K. \tag{34}$$

Expanding the Knudsen correction in an asymptotic series in ϵ,

$$\phi_K = \sum_{n=0}^{\infty} \epsilon^n \phi_K^{(n)}, \tag{35}$$

yields the governing equations,

$$v_i n_i \frac{\partial \phi_K^{(0)}}{\partial \eta} = Q_K^{(0)} - \phi_K^{(0)}, \tag{36a}$$

$$v_i n_i \frac{\partial \phi_K^{(1)}}{\partial \eta} = Q_K^{(1)} - \phi_K^{(1)}, \tag{36b}$$

$$-i\zeta\phi_K^{(n-2)} + v_i n_i \frac{\partial \phi_K^{(n)}}{\partial \eta} + v_i \left(\frac{\partial \chi_1}{\partial x_i}\frac{\partial \phi_K^{(n-2)}}{\partial \chi_1} + \frac{\partial \chi_2}{\partial x_i}\frac{\partial \phi_K^{(n-2)}}{\partial \chi_2} \right) = Q_K^{(n)} - \phi_K^{(n)}, \quad n \geq 2. \tag{36c}$$

Note that in contrast to the other regions, the leading-order distribution function, $\phi_K^{(0)}$, is no longer Maxwellian. That is, inter-particle collisions and particle collisions with the solid wall are equally important in the Knudsen layer. In addition, it is noted that, in the Knudsen region, all coordinate gradients $\frac{\partial \chi_{1,2}}{\partial x_i}$ are evaluated at $\eta = y = 0$.

The above solutions in the Hilbert, viscous, and Kundsen regions are substituted into the collision invariants, Eq. (26), the results of which are matched in their respective overlap regions that we now describe. Importantly, the Knudsen layer contributes a correction, ϕ_K, to the distribution function, ϕ, that decays to zero faster than any inverse power of η [32].

D. Matching of Hilbert and viscous regions

The Hilbert and viscous distribution functions to $O(\epsilon^2)$ are respectively,

$$\phi_H = \phi_H^{(0)} + \epsilon\phi_H^{(1)} + \epsilon^2\phi_H^{(2)} + O(\epsilon^3), \tag{37a}$$

$$\phi_V = \phi_V^{(0)} + \epsilon\phi_V^{(1)} + \epsilon^2\phi_V^{(2)} + O(\epsilon^3). \tag{37b}$$

Matching requires the inner part of the Hilbert region, $(x_i - x_{wi})n_i \equiv \epsilon y \ll 1$, to coincide with the outer part of the viscous region, $y \gg 1$. This is performed by first expanding $\phi_H^{(n)}$ with respect to the normal distance from the boundary, $(x_i - x_{wi})n_i \equiv \epsilon y$, giving

$$\phi_H^{(n)} = \left(\phi_H^{(n)} + \epsilon y n_i \frac{\partial \phi_H^{(n)}}{\partial x_i} + \frac{1}{2}(\epsilon y)^2 \left(n_i \frac{\partial}{\partial x_i} \right)^2 \phi_H^{(n)} \right)\Bigg|_{(x_i - x_{wi})n_i = 0} + O\left(\epsilon^3\right). \tag{38}$$

Substituting Eq. (38) into (37a) and collecting terms of equal order in ϵ, produces

$$\phi_H = \left(\phi_H^{(0)} + \epsilon \left(\phi_H^{(1)} + y n_i \frac{\partial \phi_H^{(0)}}{\partial x_i} \right) + \epsilon^2 \left(\phi_H^{(2)} + y n_j \frac{\partial \phi_H^{(1)}}{\partial x_j} + \frac{1}{2} y^2 \left(n_i \frac{\partial}{\partial x_i} \right)^2 \phi_H^{(0)} \right)\Bigg|_{(x_i - x_{wi})n_i = 0} \right) + O\left(\epsilon^3\right). \tag{39}$$

This expression for ϕ_H is then matched to the equivalent expression for ϕ_V with $y \gg 1$, resulting in the following asymptotic matching conditions for ϕ_V to $O(\epsilon^2)$,

$$\phi_V^{(0)}\Big|_{y\to\infty} \sim \phi_H^{(0)}\Big|_{(x_i-x_{wi})n_i\to 0}, \tag{40a}$$

$$\phi_V^{(1)}\Big|_{y\to\infty} \sim \left(\phi_H^{(1)} + yn_i\frac{\partial \phi_H^{(0)}}{\partial x_i}\right)\Bigg|_{(x_i-x_{wi})n_i\to 0}, \tag{40b}$$

$$\phi_V^{(2)}\Big|_{y\to\infty} \sim \left(\phi_H^{(2)} + yn_i\frac{\partial \phi_H^{(1)}}{\partial x_i} + \frac{1}{2}y^2\left(n_i\frac{\partial}{\partial x_i}\right)^2\phi_H^{(0)}\right)\Bigg|_{(x_i-x_{wi})n_i\to 0}. \tag{40c}$$

The corresponding moments in the viscous and Hilbert regions are matched in a similar fashion. Specific cases illustrating this matching procedure are given in the examples that follow. It is evident that the matching procedure provides an asymptotic polynomial growth condition on the viscous solutions as $y \to \infty$.

E. Knudsen correction

The Knudsen equations in Eqs. (36a) – (36c) are rewritten as

$$v_i n_i \frac{\partial \phi_K^{(n)}}{\partial \eta} + \phi_K^{(n)} = Q_K^{(n)} + R^{(n)}, \tag{41}$$

where $R^{(n)}$ is a remainder term, with $R^{(0)} = R^{(1)} = 0$. The boundary conditions for the Kundsen region are

$$\lim_{\eta\to\infty} \phi_K^{(n)} = 0, \tag{42a}$$

$$\phi_K^{(n)} = \sigma_b^{(n)} + 2V_i^{(n)}v_i + \left(v_i^2 - \frac{3}{2}\right)\tau_b^{(n)}, \qquad v_i n_i > 0. \tag{42b}$$

Eq. (41) are solved using an integrating factor to give

$$\phi_K^{(n)} = \begin{cases} e^{-\frac{\eta}{v_i n_i}}\left(\phi_b^{(n)} - Q_{V0}^{(n)} + \int_0^\eta \frac{1}{v_i n_i} e^{\frac{\eta'}{v_i n_i}}\left(Q_K^{(n)} + R^{(n)}\right)d\eta'\right), & v_i n_i > 0 \\ \int_\infty^\eta \frac{1}{v_i n_i} e^{\frac{\eta'-\eta}{v_i n_i}}\left(Q_K^{(n)} + R^{(n)}\right)d\eta', & v_i n_i < 0, \end{cases} \tag{43}$$

where $\phi_{V0} = \phi_V\big|_{y=0}$. The density, velocity and temperature corrections in the Knudsen region are specified by moments of $\phi_K^{(n)}$; a coupled set of Weiner-Hopf integral equations arise for these moments. To leading-order in ϵ, these integral equations are identical to those listed in Ref. [47]. The unique solution to the leading-order problem throughout the Knudsen region is [47, 48]

$$\phi_K^{(0)} = 0, \tag{44}$$

which gives $\phi_V^{(0)} = Q_b^{(0)}$ at the solid boundary. This produces the no-slip condition for the leading-order bulk velocity, $\bar{v}_{V|i}^{(0)}$, in the viscous region at the solid boundary. Because $\partial \bar{v}_{V|i}^{(0)} n_i/\partial y = 0$ from Table II, it then follows that $\lim_{(x_i-x_{wi})n_i\to 0} \bar{v}_{H|i}^{(0)} n_i = V_i^{(0)} n_i$, which is the no-penetration boundary condition for the leading-order Hilbert equations.

From Eqs. (36a) – (36c) and the definition of $R^{(n)}$ in Eq. (41),

$$R^{(2)} = i\zeta\phi_K^{(0)} - \epsilon^2 v_i\left(\frac{\partial \chi_1}{\partial x_i}\frac{\partial}{\partial \chi_1} + \frac{\partial \chi_2}{\partial x_i}\frac{\partial}{\partial \chi_2}\right)\phi_K^{(0)} = 0. \tag{45}$$

Application of the collision invariant, Eq. (26), with $\Phi = 1$, corresponding to mass conservation, leads to

$$\frac{\partial \bar{v}_{K|i}^{(m)} n_i}{\partial \eta} = 0, \qquad m = 0, 1, 2. \tag{46}$$

Because $\lim_{\eta\to\infty}\phi_K^{(m)}=0$, all moments of $\phi_K^{(m)}$ also vanish, giving

$$\bar{v}_{K|i}^{(m)}n_i=0,\qquad m=0,1,2. \tag{47}$$

From Eqs. (46) and (47) it then follows that the no-penetration condition at the inner part of the viscous region persists up to and including $O(\epsilon^2)$. The corresponding integral equations at $O(\epsilon)$ are identical to those reported in Refs. [34, 47]. Following the method outlined in Refs. [34, 47] gives the required slip conditions for the viscous region. A summary of the required boundary conditions for the viscous region are listed in Table III.

1. Pressure tensor and heat flux vector

Similarly, conservation of momentum and energy via Eq. (26) gives

$$\frac{\partial P_{K|ij}^{(m)}n_i}{\partial\eta}=\frac{\partial q_{K|i}^{(m)}n_i}{\partial\eta}=0,\qquad m=0,1,2. \tag{48}$$

Since all Knudsen corrections vanish in the outer part of the Knudsen region, by construction, it then follows from Eq. (48) that the normal stress correction and normal heat flux in the Knudsen region are also zero, i.e.,

$$P_{K|ij}^{(m)}n_i=q_{K|i}^{(m)}n_i=0,\qquad m=0,1,2. \tag{49}$$

This establishes that calculation of hydrodynamic forces, correct to $O(\epsilon^2)$, does not involve $P_{K|ij}^{(m)}$ for $m=0,1,2$.

The correction to the pressure tensor in the Knudsen region is then determined from the distribution function in Eq. (43), from which it follows that $P_{K|ij}^{(1)}$ and $P_{K|ij}^{(2)}$ are both diagonal, and $P_{K|ij}^{(1)}t_i^1t_j^1=P_{K|ij}^{(1)}t_i^2t_j^2$. The latter components are directly related to the first order pressure via

$$P_K^{(1)}=\sigma_K^{(1)}+\tau_K^{(1)}=\frac{1}{3}\mathrm{tr}\left(P_{K|ij}^{(1)}\right)=\frac{2}{3}P_{K|ij}^{(1)}t_i^1t_j^1, \tag{50}$$

from which it follows that

$$P_{K|ij}^{(1)}t_i^1t_j^1=P_{K|ij}^{(1)}t_i^2t_j^2=\frac{3}{2}P_K^{(1)}. \tag{51}$$

Eqs. (48) and (51) specify all components of $P_{K|ij}^{(1)}$ in the local Cartesian frame of the surface.

Calculating the remaining pressure tensor components $P_{K|ij}^{(2)}t_i^1t_j^1, P_{K|ij}^{(2)}t_i^2t_j^2$ from moments of Eq. (43) shows that they satisfy

$$\sqrt{\pi}P_{K|ij}^{(2)}t_i^2t_j^2=\sqrt{\pi}P_{K|ij}^{(2)}t_i^1t_j^1+2\left(t_i^2t_j^2\frac{\partial\chi_2}{\partial x_i}\frac{\partial\bar{v}_{V0|j}^{(0)}}{\partial\chi_2}-t_i^1t_j^1\frac{\partial\chi_1}{\partial x_i}\frac{\partial\bar{v}_{V0|j}^{(0)}}{\partial\chi_1}\right)J_0(\eta). \tag{52}$$

From their relationship to $P_K^{(2)}$, we then obtain

$$P_{K|ij}^{(2)}t_i^1t_j^1=\frac{3}{2}P_K^{(2)}+\frac{1}{\sqrt{\pi}}\left(t_i^1t_j^1\frac{\partial\chi_1}{\partial x_i}\frac{\partial\bar{v}_{V0|j}^{(0)}}{\partial\chi_1}-t_i^2t_j^2\frac{\partial\chi_2}{\partial x_i}\frac{\partial\bar{v}_{V0|j}^{(0)}}{\partial\chi_2}\right)J_0(\eta), \tag{53a}$$

$$P_{K|ij}^{(2)}t_i^2t_j^2=\frac{3}{2}P_K^{(2)}+\frac{1}{\sqrt{\pi}}\left(t_i^2t_j^2\frac{\partial\chi_1}{\partial x_i}\frac{\partial\bar{v}_{V0|j}^{(0)}}{\partial\chi_2}-t_i^1t_j^1\frac{\partial\chi_1}{\partial x_i}\frac{\partial\bar{v}_{V0|j}^{(0)}}{\partial\chi_1}\right)J_0(\eta). \tag{53b}$$

A subset of these Knudsen corrections and slip coefficients have been reported in the literature [32, 34, 47, 49]. In addition, some slip coefficients and Knudsen functions are identical because they satisfy the same governing equations, e.g.,

$$\begin{gathered}G_2=G_4=Z_0,\qquad A_3=W_0,\qquad M_2(\eta)=M_4(\eta)=M_8(\eta)=Y_1(\eta),\\ C_3(\eta)=M_5(\eta)=X_2(\eta),\qquad B_3(\eta)=X_1(\eta),\qquad M_1(\eta)=M_7(\eta).\end{gathered} \tag{54}$$

We retain the present nomenclature because it highlights the connection of these coefficients to each physical quantity; each letter symbol describes an individual slip condition or Knudsen function. Numerical values for these slip coefficients and Knudsen functions are given in Appendix B.

$\boldsymbol{n=0}$	
$\bar{v}^{(0)}_{K\|i}$	0
$\bar{v}^{(0)}_{V0\|i} - V^{(0)}_i$	0
$\tau^{(0)}_{V0} - \tau^{(0)}_b$	0
$\sigma^{(0)}_K$	0
$\tau^{(0)}_K$	0
$P^{(0)}_{K\|ij}$	0
$q^{(0)}_{K\|i}$	0
$\boldsymbol{n=1}$	
$\bar{v}^{(1)}_{K\|i} t^{1,2}_i$	$Y_1(\eta)\frac{\partial \bar{v}^{(0)}_{V0\|i} t^{1,2}_i}{\partial y}$
$(\bar{v}^{(1)}_{V0\|i} - V^{(1)}_i) t^{1,2}_i$	$Z_0 \frac{\partial \bar{v}^{(0)}_{V0\|i} t^{1,2}_i}{\partial y}$
$\bar{v}^{(1)}_{K\|i} n_i$	0
$(\bar{v}^{(1)}_{V0\|i} - V^{(1)}_i) n_i$	0
$\tau^{(1)}_{V0} - \tau^{(1)}_b$	$W_0 \frac{\partial \tau^{(0)}_{V0}}{\partial y}$
$\sigma^{(1)}_K$	$X_1(\eta)\frac{\partial \tau^{(0)}_{V0}}{\partial y}$
$\tau^{(1)}_K$	$X_2(\eta)\frac{\partial \tau^{(0)}_{V0}}{\partial y}$
$P^{(1)}_{K\|ij} n_i$	0
$P^{(1)}_{K\|ij} t^{1,2}_i t^{2,1}_j$	0
$P^{(1)}_{K\|ij} t^{1,2}_i t^{1,2}_j$	$\frac{3}{2} P^{(1)}_K$
$q^{(1)}_{K\|i} n_i$	0
$q^{(1)}_{K\|i} t^{1,2}_i$	$Y_2(\eta)\frac{\partial \bar{v}^{(0)}_{V0\|i} t^{1,2}_i}{\partial y}$
$\boldsymbol{n=2}$	
$(\bar{v}^{(2)}_{V0\|i} - V^{(2)}_i) t^{1,2}_i$	$G_1 \frac{\partial^2 \bar{v}^{(0)}_{V0\|i} t^{1,2}_i}{\partial y^2} + G_2 n_k t^{1,2}_j \frac{\partial \chi_{1,2}}{\partial x_j}\frac{\partial \bar{v}^{(0)}_{V0\|k}}{\partial \chi_{1,2}} + G_3 t^{1,2}_i \frac{\partial \chi_{1,2}}{\partial x_i}\frac{\partial \tau^{(0)}_{V0}}{\partial \chi_{1,2}} + G_4 \frac{\partial \bar{v}^{(1)}_{V0\|i} t^{1,2}_i}{\partial y}$
$\bar{v}^{(2)}_{K\|i} t^{1,2}_i$	$M_1(\eta)\frac{\partial^2 \bar{v}^{(0)}_{V0\|i} t^{1,2}_i}{\partial y^2} + M_2(\eta) n_k t^{1,2}_j \frac{\partial \chi_{1,2}}{\partial x_j}\frac{\partial \bar{v}^{(0)}_{V0\|k}}{\partial \chi_{1,2}} + M_3(\eta) t^{1,2}_i \frac{\partial \chi_{1,2}}{\partial x_i}\frac{\partial \tau^{(0)}_{V0}}{\partial \chi_{1,2}} + M_4(\eta)\frac{\partial \bar{v}^{(1)}_{V0\|i} t^{1,2}_i}{\partial y}$
$\bar{v}^{(2)}_{K\|i} n_i$	0
$(\bar{v}^{(2)}_{V0\|i} - V^{(2)}_i) n^{1,2}_i$	0
$\tau^{(2)}_{V0} - \tau^{(2)}_b$	$A_1 i\zeta \sigma^{(0)}_{V0} + A_2 i\zeta \tau^{(0)}_{V0} + W_0 \frac{\partial \tau^{(1)}_{V0}}{\partial y} + A_4 \left(\frac{\partial \chi_1}{\partial x_j}\frac{\partial}{\partial \chi_1} + \frac{\partial \chi_2}{\partial x_j}\frac{\partial}{\partial \chi_2}\right)(\bar{v}^{(0)}_{V0\|j})$
$\sigma^{(2)}_K$	$B_1(\eta) i\zeta \sigma^{(0)}_{V0} + B_2(\eta) i\zeta \tau^{(0)}_{V0} + B_3(\eta)\frac{\partial \tau^{(1)}_{V0}}{\partial y} + B_4(\eta)\left(\frac{\partial \chi_1}{\partial x_j}\frac{\partial}{\partial \chi_1} + \frac{\partial \chi_2}{\partial x_j}\frac{\partial}{\partial \chi_2}\right)(\bar{v}^{(0)}_{V0\|j})$
$\tau^{(2)}_K$	$C_1(\eta) i\zeta \sigma^{(0)}_{V0} + C_2(\eta) i\zeta \tau^{(0)}_{V0} + C_3(\eta)\frac{\partial \tau^{(1)}_{V0}}{\partial y} + C_4(\eta)\left(\frac{\partial \chi_1}{\partial x_j}\frac{\partial}{\partial \chi_1} + \frac{\partial \chi_2}{\partial x_j}\frac{\partial}{\partial \chi_2}\right)(\bar{v}^{(0)}_{V0\|j})$
$P^{(2)}_{K\|ij} n_i$	0
$P^{(2)}_{K\|ij} t^{1,2}_i t^{2,1}_j$	0
$P^{(2)}_{K\|ij} t^{1,2}_i t^{1,2}_j$	$\frac{3}{2} P^{(2)}_K + \frac{1}{\sqrt{\pi}}\left(t^{1,2}_i t^{1,2}_j \frac{\partial \chi_{1,2}}{\partial x_i}\frac{\partial \bar{v}^{(0)}_{V0\|j}}{\partial \chi_{1,2}} - t^{2,1}_i t^{2,1}_j \frac{\partial \chi_{2,1}}{\partial x_i}\frac{\partial \bar{v}^{(0)}_{V0\|j}}{\partial \chi_{2,1}}\right) J_0(\eta)$
$q^{(2)}_{K\|i} n_i$	0
$q^{(2)}_{K\|i} t^{1,2}_i$	$M_5(\eta)\frac{\partial^2 \bar{v}^{(0)}_{V0\|i} t^1_i}{\partial y^2} + M_6(\eta) n_k t^1_j \frac{\partial \chi_{1,2}}{\partial x_j}\frac{\partial \bar{v}^{(0)}_{V0\|k}}{\partial \chi_{1,2}} + M_7(\eta) t^1_i \frac{\partial \chi_{1,2}}{\partial x_i}\frac{\partial \tau^{(0)}_{V0}}{\partial \chi_{1,2}} + M_8(\eta)\frac{\partial \bar{v}^{(1)}_{V0\|i} t^1_i}{\partial y}$

TABLE III: Knudsen corrections and slip results to second order.

F. Curvature coefficients

The surface normal and geodesic principal curvatures, κ_q and g_q, respectively, where $q = 1, 2$, are [32, 46]

$$t_j^q \left(\frac{\partial \chi_q}{\partial x_j}\right)_0 \frac{\partial t_i^q}{\partial \chi_q} = t_j^q \frac{\partial t_i^q}{\partial x_j} = -\kappa_q n_i - (-1)^q g_q t_i^{3-q}, \tag{55a}$$

$$t_j^q \left(\frac{\partial \chi_q}{\partial x_j}\right)_0 \frac{\partial t_i^{3-q}}{\partial \chi_q} = t_j^q \frac{\partial t_i^{3-q}}{\partial x_j} = (-1)^q g_q t_i^q, \tag{55b}$$

$$t_j^q \left(\frac{\partial \chi_q}{\partial x_j}\right)_0 \frac{\partial n_i}{\partial \chi_q} = t_j^q \frac{\partial n_i}{\partial x_j} = \kappa_q t_i^q, \tag{55c}$$

$$t_j^q \frac{\partial \kappa_q}{\partial x_j} = -g_q(\kappa_1 - \kappa_2). \tag{55d}$$

These are used to express the governing equations for the viscous region (Table II) in a form that is more amenable to computation, while being less physically illuminating. The results of this manipulation are given in Appendix C.

G. Outline of solution process

The system of governing equations at each order, n, is closed. At leading order, $n = 0$, there is no Knudsen correction or slip condition for the viscous solution. For $n \geq 1$, the slip condition using viscous solutions of order $k < n$ provides the surface boundary condition for the viscous solution of order n. At all orders, n, use of the appropriate polynomial growth condition as $y \to \infty$ provides the other boundary conditions for the viscous region.

The Hilbert solution may be solved by applying (i) surface boundary conditions derived using the matching conditions in Section III C, and (ii) the Sommerfeld radiation condition [50] for problems involving unbounded domains. The applications that follow illustrate this solution process in detail.

IV. APPLICATIONS

We now illustrate the utility of the derived theory by applying it to several canonical examples: (i) the flow generated in a gas that is confined between two walls that undergo time dependent (oscillatory) uniform heating, (ii) oscillatory thermal creep between two walls, and (iii) the flow generated by a sphere that is oscillating in a quiescent and unbounded gas. In all cases, the flow is chosen to coincide with the acoustic regime, where the acoustic wavelength is comparable to the geometric length scale. This provides complementary examples to those of previous studies that focused on alternate flow regimes [34, 36]. Comparisons to these previous studies and numerical solution of the Boltzmann-BGK equation are also reported. We do not provide a comprehensive study of these canonical examples, but rather focus on validating the developed theory while pointing out major features of the flow. As above, the subscript 0 indicates evaluation at the wall, i.e., $\phi_{H0}^{(n)} \equiv \lim_{(x_i - x_{wi})n_i \to 0} \phi_H^{(n)}$ and $\phi_{V0}^{(n)} \equiv \lim_{y \to 0} \phi_V^{(n)}$ together with their corresponding moments.

To facilitate comparison, we form composite asymptotic solutions for each problem below by combining solutions in the viscous and Hilbert regions in the usual fashion,

$$X_C = X_H + X_V - \left(X_V|_{y \to \infty} \right), \tag{56}$$

where X is the transport variable of interest, and the subscripts V and H refer to solutions in the viscous and Hilbert regions, as above. While the composite solution, X_C, is an approximation for finite k, giving error predominantly in the (matching) overlap region between the viscous and Hilbert regions, it is exact in the required asymptotic limit, $k \to 0$. Because the solution in the Knudsen region is constructed as per Section III C, the required total composite solution follows directly from Eq. (56),

$$X_{\text{total}} = X_K + X_C. \tag{57}$$

This composite formula is used in all comparisons that follow.

A. Application 1: Antisymmetric uniform heating

We consider the gas flow generated between two stationary infinite parallel walls with oscillatory uniform temperature perturbations applied to each wall. This strictly non-continuum effect (with continuum theory predicting no flow) was studied by Manela & Hadjiconstantinou [51, 52] and Nassios, Yap & Sader [53]. Herein we consider the antisymmetric heating problem, where the temperature perturbations at both walls are equal in magnitude but opposite in sign; see Fig. 2 with boundary conditions A. By linearity, the general flow problem may be constructed from linear combinations of flows generated by antisymmetric and symmetric temperature perturbations at the walls. The following velocity and length scales are used,

$$v_s = \frac{L}{\omega}, \qquad x_s = L. \tag{58}$$

Symmetry dictates that the flow need be solved only for $0 \leq x \leq 1/2$, with temperature and density being antisymmetric and the velocity symmetric about $x = 1/2$. The wall temperature perturbations are scaled to unity. Because there is no Knudsen number dependence in these temperature boundary conditions, the components of the wall temperature at $x = 0$ are

$$\tau_b = \tau_b^{(0)} = 1, \qquad \tau_b^{(n)} = 0, \quad n \geq 1. \tag{59}$$

This flow problem is solved correct to $O(\epsilon^2)$ using the theory reported in the preceding section. Its validity is assessed by comparison to direct numerical simulations of the linearized Boltzmann-BGK equation [21].

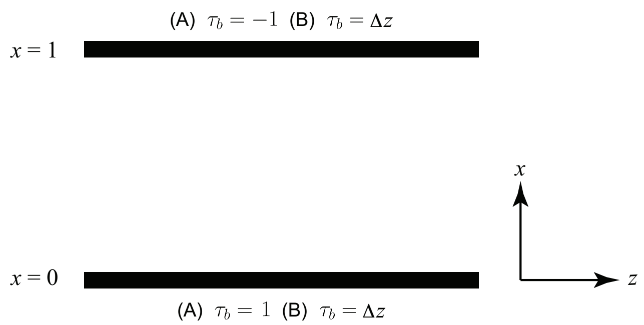

FIG. 2: Schematic for Applications 1 and 2 showing infinite parallel walls, where temperature boundary conditions are applied, that confine the gas in the region $0 \leq x \leq 1$. Two wall boundary conditions are considered: (A) Antisymmetric temperature perturbations, and (B) symmetric temperature gradients in the x-direction; these correspond to Applications 1 and 2 in Sections IV A and IV B, respectively.

1. *Leading-order solution ($n = 0$)*

The velocity equation in the (outer) Hilbert region is

$$\frac{\partial^2 \bar{v}_H^{(0)}}{\partial x^2} = -\frac{6}{5}\zeta^2 \bar{v}_H^{(0)}, \tag{60}$$

where ζ is the acoustic wavenumber defined in Eq. (18), which upon application of its no-penetration condition gives

$$\bar{v}_H^{(0)} = \tau_H^{(0)} = \sigma_H^{(0)} = P_H^{(0)} = Q_H^{(0)} = \phi_H^{(0)} = 0. \tag{61}$$

There is no Knudsen layer to leading-order ($n = 0$) and transport in the viscous region satisfies the no-slip velocity condition and temperature at the wall. By constancy of the pressure and velocity in the viscous region, normal to the wall, we obtain

$$\tau_V^{(0)} = \frac{2}{5}P_V^{(0)} + \left(1 - \frac{2}{5}P_V^{(0)}\right) e^{\sqrt{\zeta}(-1+i)y}, \qquad \bar{v}_V^{(0)} = 0, \tag{62}$$

where $y \equiv x/\epsilon$ in the present problem and $\epsilon \equiv \sqrt{k}$ is the dimensionless viscous penetration depth. Matching the above Hilbert and viscous regions then gives $P_V^{(0)} = 0$ and hence

$$\tau_V^{(0)} = -\sigma_V^{(0)} = e^{\sqrt{\zeta}(-1+i)y}, \tag{63}$$

showing that the only leading-order nonzero transport variables are the temperature and density in the viscous region.

2. First-order solution ($n = 1$)

We begin with the viscous region, for which the governing equations are

$$\frac{\partial P_V^{(1)}}{\partial y} = 2i\zeta \bar{v}_V^{(0)}, \tag{64a}$$

$$\frac{\partial \bar{v}_V^{(0)}}{\partial y} = i\zeta \sigma_V^{(0)}, \tag{64b}$$

$$\frac{\partial^2 \tau_V^{(1)}}{\partial y^2} + 2i\zeta \tau_V^{(1)} = \frac{4}{5} i\zeta P_V^{(1)}. \tag{64c}$$

Substituting Eq. (62) into Eq. (64a) shows that $P_V^{(1)}$ is constant; this constant is calculated below by matching with the Hilbert region. Solving Eqs. (64) subject to its no-penetration and slip conditions gives

$$\tau_{V0}^{(1)} = W_0\sqrt{\zeta}(-1+i), \qquad \tau_V^{(1)} = \frac{2}{5}P_V^{(1)} + \left(W_0\sqrt{\zeta}(-1+i) - \frac{2}{5}P_V^{(1)}\right) e^{\sqrt{\zeta}(-1+i)y}, \tag{65a}$$

$$\bar{v}_V^{(1)} = \frac{(1-i)\sqrt{\zeta}}{2}\left(1 - e^{\sqrt{\zeta}(-1+i)y}\right). \tag{65b}$$

In the Hilbert region, the governing equations are rewritten as

$$\frac{\partial \bar{v}_H^{(1)}}{\partial x} = i\zeta \sigma_H^{(1)}, \tag{66a}$$

$$\frac{\partial^2 \bar{v}_H^{(1)}}{\partial x^2} = -\frac{6}{5}\zeta^2 \bar{v}_H^{(1)}, \tag{66b}$$

$$\tau_H^{(1)} = \frac{2}{3}\sigma_H^{(1)}. \tag{66c}$$

with the velocity being symmetric about $x = 1/2$. The velocity in the viscous region, Eq. (65b), specifies the required boundary conditions, giving

$$\bar{v}_H^{(1)} = \frac{(1-i)\sqrt{\zeta}}{2} \frac{\cos\left(\sqrt{\frac{6}{5}}\zeta\left(x - \frac{1}{2}\right)\right)}{\cos\left(\frac{1}{2}\sqrt{\frac{6}{5}}\zeta\right)}, \tag{67}$$

from which the density and temperature follow via Eqs. (66),

$$\sigma_H^{(1)} = \sqrt{\frac{6}{5}}\frac{(1+i)\sqrt{\zeta}}{2} \frac{\sin\left(\sqrt{\frac{6}{5}}\zeta\left(x - \frac{1}{2}\right)\right)}{\cos\left(\frac{1}{2}\sqrt{\frac{6}{5}}\zeta\right)}, \qquad \tau_H^{(1)} = \frac{2}{3}\sigma_H^{(1)}, \qquad P_H^{(1)} = \frac{5}{3}\sigma_H^{(1)}. \tag{68}$$

Matching the temperatures in the Hilbert and viscous regions, Eqs. (65a) and (68), then gives

$$P_V^{(1)} = -\sqrt{\frac{5}{6}}(1+i)\sqrt{\zeta}\tan\left(\frac{1}{2}\sqrt{\frac{6}{5}}\zeta\right). \tag{69}$$

The first-order Knudsen corrections are found from the leading-order solutions in the viscous region (Section IV A 1), giving

$$\tau_K^{(1)} = \sqrt{\zeta}(-1+i)\sum_{m=0}^{7} x_{2,m}J_m(\eta), \qquad \sigma_K^{(1)} = \sqrt{\zeta}(-1+i)\sum_{m=0}^{7} x_{1,m}J_m(\eta), \qquad v_K^{(1)} = 0, \tag{70}$$

where for this problem, $\eta \equiv x/\epsilon^2$ (see Eq. (33)).

3. Second-order solution ($n = 2$)

The governing equations in the viscous region are

$$\frac{\partial \bar{v}_V}{\partial y} = i\sigma_V^{(1)}, \tag{71a}$$

$$\frac{\partial P_V^{(2)}}{\partial y} = 2i\zeta \bar{v}_V^{(1)}, \tag{71b}$$

$$\frac{\partial^2 \tau_V^{(2)}}{\partial y^2} + 2i\zeta\tau_V^{(2)} = \frac{4}{5}i\zeta P_V^{(2)} + \frac{11}{5}i\zeta\frac{\partial^2 \tau_V^{(0)}}{\partial y^2}. \tag{71c}$$

Solving Eqs. (71) subject to the no-penetration conditions gives

$$\bar{v}_V^{(2)} = \frac{3}{5}i\zeta P_V^{(1)} y + \left(-i\zeta W_0 + \frac{1}{5}\sqrt{\zeta}P_V^{(1)}(1-i)\right)\left(e^{\sqrt{\zeta}(-1+i)y} - 1\right), \tag{72a}$$

$$P_V^{(2)} = \zeta\sqrt{\zeta}(1+i)y + i\zeta(e^{\sqrt{\zeta}(-1+i)y} - 1) + p_0, \tag{72b}$$

where p_0 is a constant (to be evaluated by matching to the Hilbert region). The temperature equation, Eq. (71c), then gives

$$\tau_V^{(2)} = e^{\sqrt{\zeta}(-1+i)y}\left(\xi - \frac{9}{10}\zeta\sqrt{\zeta}(1+i)y\right) + \frac{2}{5}\zeta\sqrt{\zeta}(1+i)y - \frac{2}{5}i\zeta + \frac{2}{5}p_0, \tag{73}$$

where

$$\xi = \tau_{V0}^{(2)} + \frac{2}{5}i\zeta - \frac{2}{5}p_0. \tag{74}$$

Because the leading order Hilbert moments vanish, the governing equations in the Hilbert region are rewritten as

$$\frac{\partial \bar{v}_H^{(2)}}{\partial x} = i\zeta\sigma_H^{(2)}, \tag{75a}$$

$$\frac{\partial^2 \bar{v}_H^{(2)}}{\partial x^2} = -\frac{6}{5}\zeta^2 \bar{v}_H^{(2)}, \tag{75b}$$

$$\tau_H^{(2)} = \frac{2}{3}\sigma_H^{(2)}. \tag{75c}$$

Solving Eqs. (75) gives

$$\bar{v}_H^{(2)} = A\cos\left(\sqrt{\frac{6}{5}}\zeta\left(x - \frac{1}{2}\right)\right), \qquad \sigma_H^{(2)} = iA\sqrt{\frac{6}{5}}\zeta\sin\left(\sqrt{\frac{6}{5}}\zeta\left(x - \frac{1}{2}\right)\right), \tag{76a}$$

$$\tau_H^{(2)} = \frac{2}{3}\sigma_H^{(2)}, \qquad P_H^{(2)} = \frac{5}{3}\sigma_H^{(2)}, \tag{76b}$$

where A is another constant to be evaluated by matching.

From Eq. (40c) it follows that

$$\phi_V^{(2)}\Big|_{y\to\infty} \sim \left(\phi_H^{(2)} + yn_i\frac{\partial \phi_H^{(1)}}{\partial x_i} + \frac{1}{2}y^2\left(n_i\frac{\partial}{\partial x_i}\right)^2 \phi_H^{(0)}\right)\Bigg|_{(x_i - x_{wi})n_i \to 0}. \tag{77}$$

Given that $\phi_H^{(0)} = 0$, Eq. (77) reduces to

$$\phi_V^{(2)}\Big|_{y\to\infty} \sim \left(\phi_H^{(2)} + yn_i\frac{\partial \phi_H^{(1)}}{\partial x_i}\right)\Bigg|_{(x_i - x_{wi})n_i \to 0}. \tag{78}$$

Matching the constant terms in the pressure gives

$$p_0 = i\zeta - \frac{5}{3} iA\sqrt{\frac{6}{5}}\zeta \sin\left(\frac{1}{2}\sqrt{\frac{6}{5}}\zeta\right), \tag{79}$$

and similarly for the velocities yields

$$A = \left(i\zeta W_0 + \frac{1}{5}\sqrt{\zeta} P_V^{(1)}(-1+i)\right) \sec\left(\frac{1}{2}\sqrt{\frac{6}{5}}\zeta\right). \tag{80}$$

The Knudsen corrections follow from Table III,

$$\tau_{V0}^{(2)} = A_1 i\zeta\sigma_V^{(0)} + A_2 i\zeta\tau_V^{(0)} + A_3 \left.\frac{\partial \tau_V^{(1)}}{\partial y}\right|_{y=0}, \tag{81a}$$

$$\sigma_K^{(2)} = \sum_{k=0}^{7}\left.\left(J_k(\eta)\left(b_{1,k}\sigma_V^{(0)} + b_{2,k}\tau_V^{(0)} + b_{3,k}\frac{\partial \tau_V^{(1)}}{\partial y}\right)\right)\right|_{y=0}, \tag{81b}$$

$$\tau_K^{(2)} = \sum_{k=0}^{7}\left.\left(J_k(\eta)\left(c_{1,k}\sigma_{V0}^{(0)} + c_{2,k}\tau_V^{(0)} + c_{3,k}\frac{\partial \tau_V^{(1)}}{\partial y}\right)\right)\right|_{y=0}, \tag{81c}$$

where the coefficients $b_{n,k}$ and $c_{n,k}$ are defined in Tables V – VI.

4. Comparison to numerical solutions of the Boltzmann-BGK equation

We now compare the above asymptotic solutions for the transport variables to direct and accurate numerical solutions of the linearized Boltzmann-BGK equation, that employ a spectral method based on the variational formulation reported by Ladiges and Sader (2018) [21]. These spectral solutions are systematically refined to achieve high accuracy and are referred to as 'exact numerical solutions' in the following discussion. In this validation study, we choose $\tau_b = 1$ and $\zeta = 1$ corresponding to the required acoustic regime.

Numerical solution: As per the examples studied in Ref. [21], the present problem consists of a bounded domain with a single spatial dimension. The approach for discretizing the Boltzmann-BGK equation (Eq. (13)) in space is therefore unchanged—a second-order finite difference method is used based on a uniform grid, that is upwinded in the direction of the particle velocity components. A spectral approach is used to discretize the particle velocity variables. Following Ref. [21], polynomial basis functions are used that have support on either $v_x > 0$ or $v_x < 0$. This allows for accurate integration of the discontinuity expected at $v_x = 0$. The basis functions cover all three particle velocity dimensions, and by symmetry we may discard polynomials which are anti-symmetric in y and z (here, y refers to the Cartesian coordinate normal to x and z, rather than the rescaled normal coordinate which is used elsewhere). While the (isothermal and constant density) examples in Ref. [21] applied a shear velocity boundary condition, here the temperature boundary condition in Eq. (59) is used. Because the flow is not of uniform density, we also enforce mass conservation at the boundary with Eq. (15). Numerical results are converged by systematically doubling the number of points in the spatial grid, and increasing the order of the basis functions in particle velocity space by two, until the relative change in all transport variables is less than 1%. Results are given for 10,000 spatial points and polynomials of order 8.

Figure 3 shows the results of this comparison for a Knudsen number of $k = 0.00625$ ($\ll 1$), i.e., $\epsilon = \sqrt{k} = 0.08$, which highlights the accuracy and validity of the developed asymptotic theory; similar agreement is found for other small values of k (data not shown). Two distinct theoretical calculations are given, with the asymptotic theory calculated correct to $O(\epsilon)$ and $O(\epsilon^2)$, using the formulas given above. Continuum theory predicts no flow for this problem, which is reflected in the vanishing leading-order velocity in the Hilbert solution, i.e., to $O(1)$. Only the density and temperature distribution are $O(1)$. Temperature gradients are confined to the viscous region, $x \lesssim \epsilon$ $(= 0.08)$, which in turn drives flow at $O(\epsilon)$ with nonzero contributions in all regions. We note that the length scale for variations in all transport parameters is inversely proportional to the acoustic wavenumber, ζ, which reflects the intrinsically compressible nature of these flows.

It is evident from Fig. 3 that the temperature and density distributions are accurately predicted by the asymptotic theory correct to $O(\epsilon)$ and $O(\epsilon^2)$. This is not surprising because these transport variables exhibit nonzero contributions at $O(1)$, as discussed above. Thus, the $O(\epsilon)$ and $O(\epsilon^2)$ corrections provide small contributions at this small value of $\epsilon = 0.08$. The same is not true for the velocity and pressure, that are $O(\epsilon)$, which we now discuss.

The $O(\epsilon)$ asymptotic solution in Section IV A 2 captures the dominant features of both the velocity and pressure, albeit with some minor quantitative differences. Inclusion of the $O(\epsilon^2)$ accurately accounts for these minor differences and gives excellent agreement with high-accuracy numerical solutions. The viscous region, $x \lesssim 0.08$, is evident in all results in Fig. 3, along with Knudsen corrections that occur within a distance of $O(\epsilon^2)$ from the wall, i.e., $x \lesssim 0.00625$. These Knudsen corrections are clearly evident in the pressure distributions to $O(\epsilon)$. Interestingly, the $O(\epsilon^2)$ correction is significant in the viscous and Hilbert regions for the velocity and pressure and must be included to accurately determine them, even at this small Knudsen number of $k = 0.00625$.

For reference, Fig. 4 compares the exact numerical solution reported in Fig. 3 to the predictions of the linearized compressible NSF set of equations with (i) no temperature-jump, and (ii) a temperature jump included. Importantly, while the solution calculated from the NSF system of equations with temperature jump provides a solution that captures the velocity, density and temperature with a similar degree of accuracy to the developed $O(\epsilon^2)$ asymptotic theory (nearly coinciding with the exact numerical solution), it misses key features of the pressure. The nonlinear structure of the pressure in the viscous region is not captured, in contrast to the developed asymptotic theory. This suggests that the derived NSF system of equations are correct to $O(\epsilon^2)$ in the Hilbert region only, not the viscous region, and thus miss pertinent features of the flow in the viscous region.

Navier-Stokes-Fourier equations (NSF) [41]: The NSF system of equations used in all benchmarking are the linearized and Fourier-transformed form of Eqs. (50a)–(50c) in Ref. [41],

$$i\zeta\sigma = \frac{\partial v_j}{\partial x_j}, \tag{82a}$$

$$i\zeta v_j = \frac{1}{2}\frac{\partial P}{\partial x_j} - \frac{1}{2}\epsilon^2\left(\frac{1}{3}\frac{\partial}{\partial x_j}\left(\frac{\partial v_w}{\partial x_w}\right) + \frac{\partial^2 v_j}{\partial {x_w}^2}\right), \tag{82b}$$

$$i\zeta\tau = \frac{2}{3}i\zeta\sigma - \frac{5}{6}\epsilon^2\frac{\partial^2\tau}{\partial {x_j}^2}, \tag{82c}$$

with associated boundary conditions at the solid walls given by Eqs. (124a)-(124c) of Ref. [41],

$$(v_i - V_i)n_i = 0, \tag{83a}$$

$$(v_i - V_i)t_i = \epsilon\left(1.01619\left(\frac{\partial v_i}{\partial x_j} + \frac{\partial v_j}{\partial x_i}\right)n_i t_j + 0.38316\frac{\partial T}{\partial x_i}t_i\right), \tag{83b}$$

$$\tau - \tau_b = \epsilon\left(1.30272\frac{\partial T}{\partial x_i}n_i + 0.44045\frac{\partial v_i}{\partial x_j}n_i n_j\right), \tag{83c}$$

where n_i is the outward wall-normal [defined in Eq. (27)] and t_i is the corresponding tangential unit vector at the wall; only one tangential vector exists because the problem is two-dimensional.

For the present application, this system of equations reduces to

$$i\zeta\sigma = \frac{dv}{dx}, \tag{84a}$$

$$i\zeta v = \frac{1}{2}\frac{dP}{dx} - \frac{2}{3}\epsilon^2\frac{d^2v}{dx^2}, \tag{84b}$$

$$i\zeta\tau = \frac{2}{3}i\zeta\sigma - \frac{5}{6}\epsilon^2\frac{d^2\tau}{dx^2}, \tag{84c}$$

with wall boundary conditions,

$$(v - V)|_{x=0,1} = 0, \tag{85a}$$

$$\tau - \tau_b = \epsilon\left(1.30272\,(-1)^x\frac{dT}{dx} + 0.44045\frac{dv}{dx}\right)\bigg|_{x=0,1}, \tag{85b}$$

where $(-1)^x$ accounts for reversal in the outward wall-normal direction at $x = 0, 1$.

Note that Eq. (84c) provides the linearized adiabatic relationship between temperature and density, with a non-continuum thermal dissipation term. Therefore, the flow is driven by thermal gradients at the wall via mass conservation, and so a flow can result even in the absence of a wall temperature jump.

Acoustic resonances: The $O(\epsilon)$ solutions in Section IV A 2 predict the expected acoustic phenomenon of resonance, which occurs when

$$\cos\left(\frac{1}{2}\sqrt{\frac{6}{5}}\zeta\right) = 0, \tag{86}$$

giving

$$\zeta_{\text{resonance}} = (2n-1)\,\pi\sqrt{\frac{5}{6}}, \tag{87}$$

where $n = 1, 2, 3, \ldots$. Equations (17), (18), and (87) establish that the characteristic gas velocity for these standing waves is $\sqrt{5/6}\,v_{mp}$. At these resonances, the present asymptotic solution yields singularities in the transport variables. This is because an asymptotic expansion is performed first with respect to k (equivalently, $\sqrt{\epsilon}$). Regularization of these singularities is most conveniently performed by combining the viscous and Hilbert regions, e.g., through use of the compressible NSF equations, as suggested in Refs. [41, 43]. Away from resonance, the $O(\epsilon)$ (non-continuum) Hilbert moments vary as $\sqrt{\zeta}$ in magnitude.

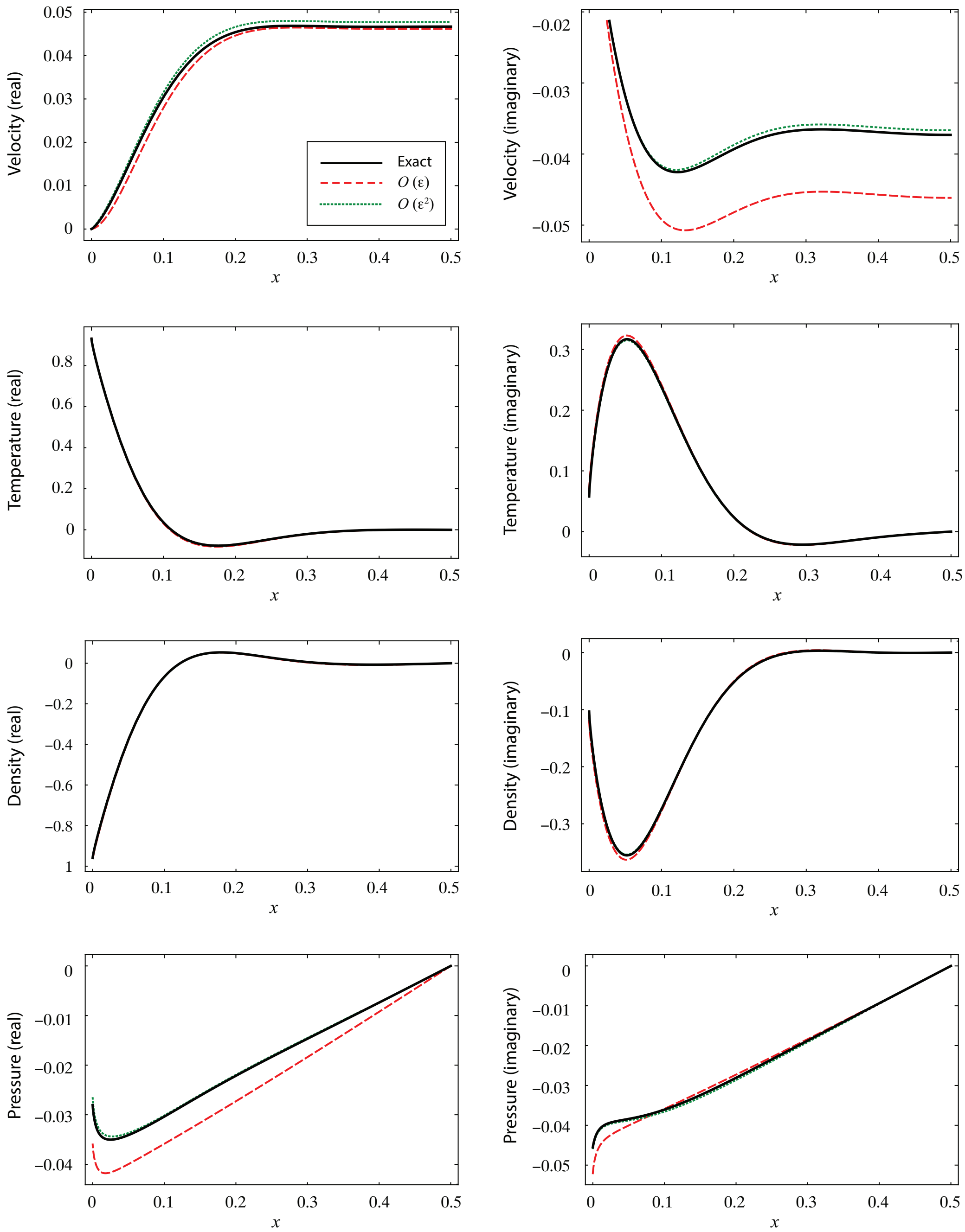

FIG. 3: Application 1: Antisymmetric uniform heating. Comparison of the exact numerical solution (solid line – black), asymptotic theory correct to $O(\epsilon)$ (dashed line – red) and asymptotic theory correct to $O(\epsilon^2)$ (dotted line – green). Results shown for $\zeta = 1$ and $k = 0.00625$. Some curves overlap with the exact numerical solution (solid line – black) and therefore are not visible.

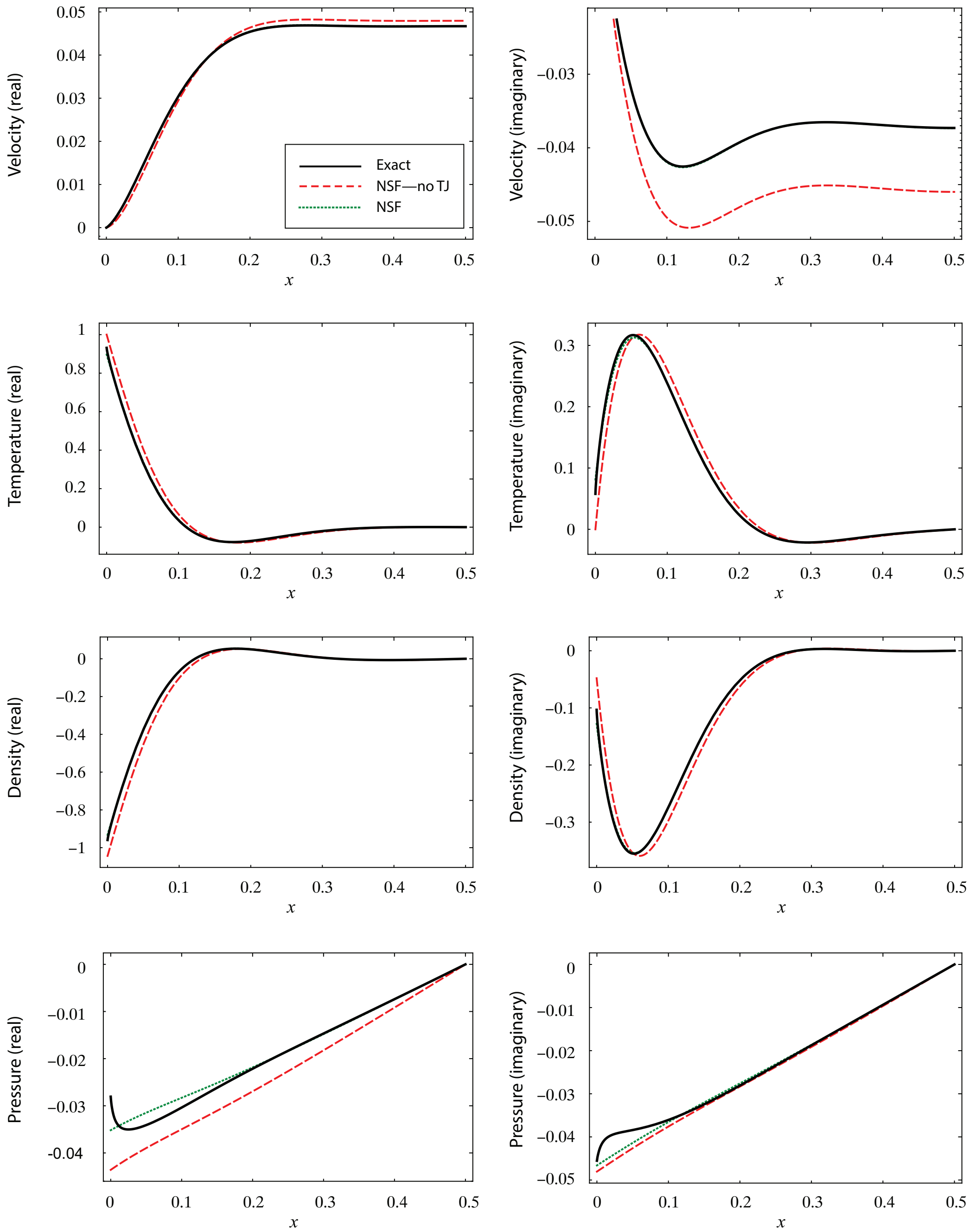

FIG. 4: Application 1: Antisymmetric uniform heating. Comparison of the exact numerical solution (solid line – black), NSF with no temperature jump (NSF—no TJ) (dashed line – red) and NSF with temperature jump (NSF) (dotted line – green). Results shown for $\zeta = 1$ and $k = 0.00625$. Some curves overlap with the exact numerical solution (solid line – black) and therefore are not visible.

B. Application 2: Oscillatory thermal creep

Next, we study the oscillatory thermal creep flow generated by temperature gradients imposed on two parallel walls separated by a distance L that confine a gas; see Fig. 2 with boundary conditions B. A uniform and oscillatory (time dependent) temperature gradient, A, is applied to each wall and the equilibrium gas temperature is T_0. The corresponding dimensionless temperature at each wall is

$$\tau_b = \Delta z, \tag{88}$$

where z is the dimensionless Cartesian coordinate (scaled by L) parallel to the walls, and

$$\Delta \equiv \frac{A}{LT_0}, \tag{89}$$

is the dimensionless temperature gradient. The dimensionless Cartesian coordinate normal to the walls is x (scaled by L), and by symmetry we only consider $0 \leq x \leq 1/2$; this specifies the flow in the entire domain. The temperature, density and tangential velocities are symmetric about $x = 1/2$ while the velocity normal to the walls is antisymmetric. The normal coordinate in the viscous region is $y \equiv x/\epsilon$, while that in the Knudsen region is $\eta \equiv x/\epsilon^2$. The Cartesian coordinate (scaled by L) parallel to the wall is $z = \chi_1$.

This strictly non-continuum flow was studied by Nassios & Sader [34] in the low frequency regime (long acoustic wavelength, $\zeta \ll 1$), where a quasi-incompressible flow is generated. Numerical results of this previous theory are compared to the present theory which is solved correct to $O(\epsilon^2)$. In a follow up study, Nassios & Sader [36] considered the high frequency (short acoustic wavelength, $\zeta \gg 1$) limit which is not compared here.

1. Leading-order solution ($n = 0$)

Analysis of the (outer) Hilbert region is identical to Application 1, and gives

$$\bar{v}_H^{(0)} = \tau_H^{(0)} = \sigma_H^{(0)} = P_H^{(0)} = Q_H^{(0)} = \phi_H^{(0)} = 0, \tag{90}$$

along with $P_V^{(0)} = 0$ for the viscous region (upon matching). The temperature equation in the viscous region then becomes

$$\frac{\partial^2 \tau_V^{(0)}}{\partial y^2} + 2i\zeta\tau_V^{(0)} = 0, \tag{91}$$

which upon application of the boundary conditions in Eq. (88) gives the required solution

$$\tau_V^{(0)} = -\sigma_V^{(0)} = \Delta z e^{\sqrt{\zeta}(-1+i)y}. \tag{92}$$

The normal and tangential velocity fields in the viscous region vanish because the walls are stationary, and there is no contribution from the Knudsen region.

2. First-order solution ($n = 1$)

We begin with the Knudsen corrections, which are determined directly from the leading-order solution in the viscous region via Table III,

$$\sigma_K^{(1)} = \Delta z\sqrt{\zeta}(-1+i)\sum_{m=0}^{n} x_{1,m} J_m(\eta), \tag{93a}$$

$$\tau_K^{(1)} = \Delta z\sqrt{\zeta}(-1+i)\sum_{m=0}^{n} x_{2,m} J_m(\eta), \tag{93b}$$

$$\bar{v}_{K|i}^{(1)} = 0. \tag{93c}$$

Next, we turn to the viscous region where the normal velocity satisfies

$$\frac{\partial \bar{v}_{V|i}^{(1)} n_i}{\partial y} = i\zeta\sigma_V^{(0)}, \tag{94}$$

whose solution is

$$\bar{v}_{V|i}^{(1)} n_i = \frac{(-1+i)\sqrt{\zeta}\Delta z}{2}\left(e^{\sqrt{\zeta}(-1+i)y} - 1\right), \tag{95}$$

while the pressure is independent of the normal coordinate, y, i.e.,

$$P_V^{(1)} = f(z), \tag{96}$$

where the function $f(z)$ is to be determined.

Because the leading-order tangential velocity vanishes, the tangential velocity in the viscous region obeys the no-slip condition, giving

$$\bar{v}_{V|i}^{(1)} t_i^1 = \frac{f'(z)}{2i\zeta}\left(1 - e^{\sqrt{\zeta}(-1+i)y}\right). \tag{97}$$

The temperature jump condition in the viscous region follows directly from the leading-order temperature,

$$\tau_{V0}^{(1)} = -W_0\sqrt{\zeta}(-1+i)\Delta z, \tag{98}$$

from which the corresponding temperature and density equations are solved to give

$$\tau_V^{(1)} = \frac{2}{5}f(z)\left(1 - e^{\sqrt{\zeta}(-1+i)y}\right) - W_0\sqrt{\zeta}(-1+i)\Delta z e^{\sqrt{\zeta}(-1+i)y}, \tag{99a}$$

$$\sigma_V^{(1)} = \frac{2}{5}f(z)\left(\frac{3}{2} + e^{\sqrt{\zeta}(-1+i)y}\right) + W_0\sqrt{\zeta}(-1+i)\Delta z e^{\sqrt{\zeta}(-1+i)y}. \tag{99b}$$

Finally, we solve the (outer) Hilbert region for which the matching conditions in Eqs. (40) become

$$\bar{v}_{H0|i}^{(1)} n_i = \frac{(1-i)\sqrt{\zeta}\Delta z}{2}, \qquad \bar{v}_{H0|i}^{(1)} t_i^1 = \frac{f'(z)}{2i\zeta}, \qquad \sigma_{H0}^{(1)} = \frac{3}{5}f(z). \tag{100}$$

The density satisfies the two-dimensional Helmholtz equation,

$$\frac{\partial^2 \sigma_H^{(1)}}{\partial x^2} + \frac{\partial^2 \sigma_H^{(1)}}{\partial z^2} + \frac{6}{5}\zeta^2 \sigma_H^{(1)} = 0, \tag{101}$$

with boundary conditions,

$$\frac{\partial \sigma_H^{(1)}}{\partial x} = \frac{3(1+i)\zeta\sqrt{\zeta}}{5}\Delta z \qquad \text{for} \quad x = 0, \tag{102a}$$

$$\frac{\partial \sigma_H^{(1)}}{\partial x} = 0 \qquad \text{for} \quad x = \frac{1}{2} \tag{102b}$$

Searching for a solution of the form, $\sigma_H^{(1)} = zg(x)$, then gives the required result,

$$\sigma_H^{(1)} = \sqrt{\frac{3}{10}}\,\frac{(1+i)\sqrt{\zeta}}{\sin\left(\frac{1}{2}\sqrt{\frac{6}{5}}\zeta\right)}\Delta z \cos\left(\sqrt{\frac{6}{5}}\zeta\left(x - \frac{1}{2}\right)\right). \tag{103}$$

from which it follows that

$$\tau_H^{(1)} = \sqrt{\frac{2}{15}}\,\frac{(1+i)\sqrt{\zeta}}{\sin\left(\frac{1}{2}\sqrt{\frac{6}{5}}\zeta\right)}\Delta z \cos\left(\sqrt{\frac{6}{5}}\zeta\left(x - \frac{1}{2}\right)\right), \tag{104a}$$

$$\bar{v}_{H|i}^{(1)} n_i = \frac{(-1+i)\sqrt{\zeta}}{2\sin\left(\frac{1}{2}\sqrt{\frac{6}{5}}\zeta\right)}\Delta z \sin\left(\sqrt{\frac{6}{5}}\zeta\left(x - \frac{1}{2}\right)\right), \tag{104b}$$

$$\bar{v}_{H|i}^{(1)} t_i^1 = \sqrt{\frac{5}{24\,\zeta}}\,\frac{(1-i)}{\sin\left(\frac{1}{2}\sqrt{\frac{6}{5}}\zeta\right)}\Delta \cos\left(\sqrt{\frac{6}{5}}\zeta\left(x - \frac{1}{2}\right)\right), \tag{104c}$$

and

$$f(z) = \sqrt{\frac{5}{6}}(1+i)\sqrt{\zeta}\Delta z \cot\left(\frac{1}{2}\sqrt{\frac{6}{5}}\zeta\right). \tag{105}$$

3. Comparison to present acoustic theory to long wavelength theory

We first highlight the key difference between the present acoustic theory and the long wavelength theory of Nassios & Sader [34]:

Nassios & Sader: Ref. [34] performed an asymptotic expansion in k under the assumption that the Stokes number, β, defined in Eq. (19), is $O(1)$. It then follows from Eq. (18) that the acoustic wavenumber, ζ, is $O(k)$, which is infinitesimally small in the asymptotic limit of small k. That is, acoustic effects are implicitly suppressed in this long wavelength limit.

Present theory: The present theory assumes that the acoustic wavenumber, ζ, is $O(1)$. This produces a Stokes number, $\beta = O(1/k)$, which is large in the asymptotic limit of small k. Acoustic effects are rigorously included in this theory.

Consequently, these two asymptotic theories apply to different flow regimes that can be expected to overlap when the acoustic wavenumber is not too large, i.e., $\zeta = O(1)$. Here, we explore this potential overlap by choosing a small but finite Kundsen number, k, and by varying the acoustic wave number, ζ. We choose a Knudsen number of $k = 0.004$ and present results for the flow field at a position $z = 1$ throughout. Numerical results are given for acoustic wavenumbers of $\zeta = 0.1, 1, 10$, which span the long to short wavelength regimes, respectively. We focus our attention on the velocity field which is the transport variable of primary interest in many applications of the thermal creep phenomenon, e.g., the Knudsen pump in microfluidic applications.

The long wavelength theory involves an asymptotic expansion in k, whereas the present acoustic theory is expanded in $\epsilon \equiv \sqrt{k}$. We compare the leading order (nonzero) contributions of both theories for this oscillatory thermal creep flow, which amounts to the long wavelength theory being calculated correct to $O(k)$ and the present theory correct to $O(\sqrt{k})$. Details of the long wavelength solution for oscillatory thermal creep are given in Ref. [34].

Figures 5 and 6 give numerical results derived from these complementary theories for the normal and tangential velocity fields, respectively. For the lowest wavenumber, $\zeta = 0.1$, these theories give quantitatively similar results for the normal velocity while exhibiting subtle differences in the velocity profiles. However, the same is not true for the tangential velocity, with the present theory dramatically overestimating the long wavelength theory of Nassios & Sader; see Fig. 6. The reason for this discrepancy is that the present theory exhibits a $1/\sqrt{\zeta}$ divergence in the long wavelength (small ζ) limit, which clearly cannot hold in that regime. This is not an issue because the present theory is not derived for that limit, but serves to highlight the different flow physics in the long wavelength (quasi-incompressible) and finite wavelength (acoustic) regimes.

Increasing the acoustic wavenumber to $\zeta = 1$ yields excellent agreement for the normal velocity, while the tangential velocities exhibit similar profiles with a quantitative difference in magnitude of order $1.5 - 2$. The large two order-of-magnitude discrepancy in the tangential velocity for $\zeta = 0.1$ no longer exists, supporting the above conclusion that the $1/\sqrt{\zeta}$ variation in the tangential velocity is strictly an acoustic phenomenon.

Operation in the strongly acoustic regime when $\zeta = 10$ gives marked differences between the two theories. This small acoustic wavelength is clearly visible in the present theory, but absent in the long wavelength (quasi-incompressible) theory of Nassios & Sader. Again, such a deviation in agreement is to be expected because the theory in Ref. [34] does not include acoustic effects.

This comparison shows the overlap of these complementary asymptotic theories for near incompressible flows, and provides some guidance as to their respective regimes of applicability. We refrain from further analysis and comparison because our primary aim here is to validate the present theory.

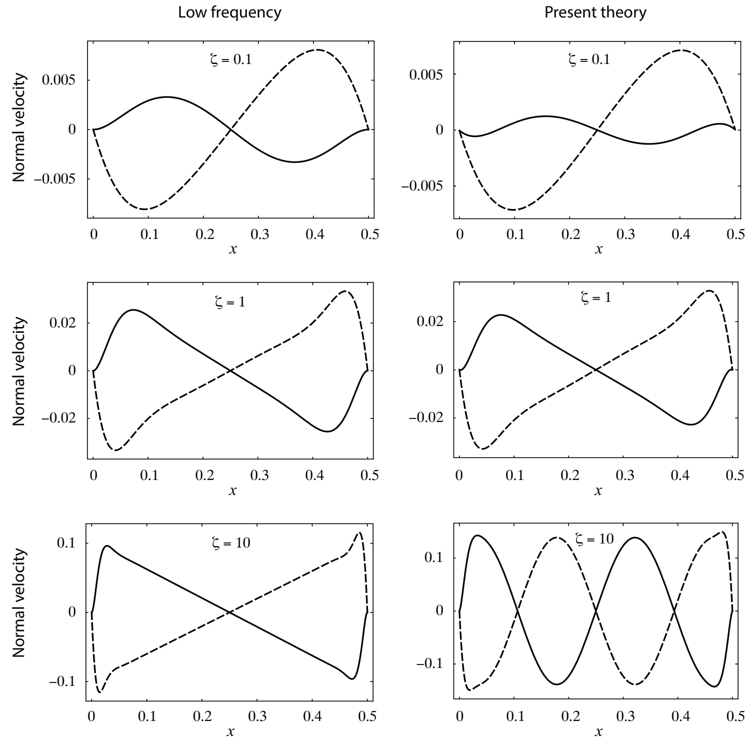

FIG. 5: Application 2: Oscillatory thermal creep. Comparison of normal velocities calculated using the theory of Nassios & Sader [34] (left) and the present asymptotic theory (right). Real component (solid line); Imaginary component (dashed line). Results shown for $k = 0.004$.

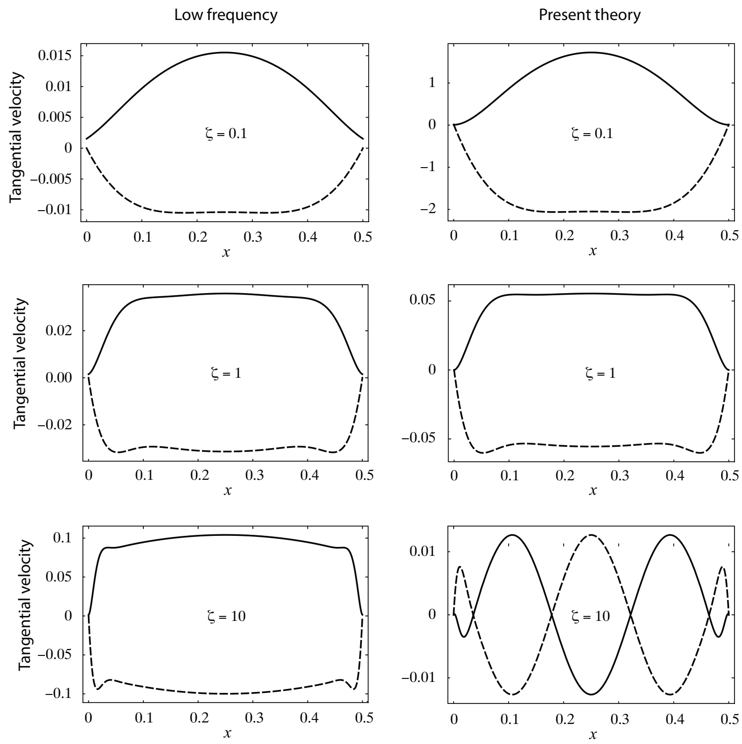

FIG. 6: Application 2: Oscillatory thermal creep. Comparison of tangential velocities calculated using the theory of Nassios & Sader [34] (left) and the present asymptotic theory (right). Real component (solid line); Imaginary component (dashed line). Results shown for $k = 0.004$.

C. Application 3: Sphere oscillating in a quiescent gas

We conclude by studying the acoustic flow generated by a solid sphere that is executing rectilinear oscillations in an otherwise quiescent and unbounded gas. In contrast to the preceding applications, an axisymmetric flow is generated. The flow is calculated using the present asymptotic theory and compared to numerical solutions of the linearized Boltzmann-BGK equation [21] to demonstrate the theory's utility in a curvilinear coordinate system. Details of this numerical solution are provided below.

The solid sphere executes rectilinear oscillations such that the dimensionless velocity of its surface (scaled by U, the sphere's dimensional speed) is

$$\mathbf{V}_s = \exp(-i\omega t)\,\hat{\mathbf{z}}, \tag{106}$$

where the sphere's surface temperature is fixed at $\tau_b \exp(-i\omega t)$, where τ_b is a position-independent constant. This corresponds to uniform heating and cooling of the surface in synchrony with the sphere's motion. The practical case where the surface is held at the ambient gas temperature coincides with $\tau_b = 0$ (which we study numerically below). These chosen velocity and temperature boundary conditions are independent of Knudsen number. All spatial dimensions are scaled by the sphere radius.

With respect to the (dimensionless) spherical polar coordinate system, (r, θ, ϕ), it follows that $t^1 = \hat{\theta}, t^2 = \hat{\phi}, \chi_1 = \theta, \chi_2 = \phi$. Expressing the radial coordinate as $r = 1 + \epsilon y$, gives the required curvature coefficients, defined in Section III F,

$$h_1 = 1 + \epsilon y, \qquad h_2 = (1 + \epsilon y)\sin\theta, \qquad \kappa_1 = \kappa_2 = 1, \qquad g_1 = 0, \qquad g_2 = \cot\theta, \tag{107}$$

where h_1 and h_2 are scale factors.

We now use the present asymptotic theory to calculate the resulting flow field correct to $O(\epsilon^2)$.

1. Leading-order solution $(n = 0)$

There is no Knudsen layer to leading order, $O(1)$. The leading order pressure and normal velocity in the viscous region are independent of the normal coordinate, $y \equiv x/\epsilon$. Therefore, the velocity boundary conditions at $y = 0$ are

$$\bar{v}^{(0)}_{V0|i} n_i = \cos\theta, \qquad \bar{v}^{(0)}_{V0|i} t^1_i = -\sin\theta, \tag{108}$$

from which it follows that the normal velocity in the viscous region is

$$\bar{v}^{(0)}_{V|i} n_i = \cos\theta. \tag{109}$$

Solutions to the temperature and density perturbations are

$$\tau^{(0)}_V = \frac{2}{5} P^{(0)}_V + \left(\tau_b - \frac{2}{5} P^{(0)}_V\right) e^{\sqrt{\zeta}(-1+i)y}, \tag{110a}$$

$$\sigma^{(0)}_V = \frac{3}{5} P^{(0)}_V - \left(\tau_b - \frac{2}{5} P^{(0)}_V\right) e^{\sqrt{\zeta}(-1+i)y}, \tag{110b}$$

where the pressure, $P^{(0)}_V$, depends only on the polar coordinate, θ, and is to be determined, i.e., $P^{(0)}_V$ is independent of y.

Noting that the above scale factors gives the following reduced form for the tangential momentum equation,

$$\frac{\partial^2 \bar{v}^{(0)}_{V|i} t^1_i}{\partial y^2} + 2i\zeta \bar{v}^{(0)}_{V|i} t^1_i = \frac{\partial P^{(0)}_V}{\partial \theta}. \tag{111}$$

Applying the boundary conditions on the spatial domain then yields

$$\bar{v}^{(0)}_{V|i} t^1_i = B e^{\sqrt{\zeta}(-1+i)y} \sin\theta - (1 + B)\sin\theta, \tag{112a}$$

$$P^{(0)}_V = 2i\zeta(1 + B)\cos\theta + c, \tag{112b}$$

where B, c are integration constants to be evaluated by matching with the Hilbert region.

We now examine the Hilbert region, where the continuity equation is

$$\frac{\partial^2 \sigma_H^{(0)}}{\partial {x_i}^2} + \frac{6}{5}\zeta^2 \sigma_H^{(0)} = 0, \tag{113}$$

which is a Helmholtz equation, whose general axisymmetric solution is

$$\sigma_H^{(0)} = \sum_{l=0}^{\infty} P_l(\cos\theta) \left(a_l j_l \left(\sqrt{\frac{6}{5}}\zeta r \right) + b_l y_l \left(\sqrt{\frac{6}{5}}\zeta r \right) \right), \tag{114}$$

where P_l are Legendre polynomials of order, l, and j_l, y_l are spherical Bessel functions of the first and second kind, respectively, again of order l. Because the density is proportional to the pressure in the Hilbert region, matching the pressure in the Hilbert and viscous regions gives

$$\sigma_{H0}^{(0)} = \frac{3}{5} P_V^{(0)} = \frac{6}{5} i\zeta(1+B)\cos\theta + \frac{3}{5}c, \tag{115}$$

by which it follows from Eq. (114) that

$$\sigma_H^{(0)} = a_0 j_0 \left(\sqrt{\frac{6}{5}}\zeta r \right) + b_0 y_0 \left(\sqrt{\frac{6}{5}}\zeta r \right) + \left[a_1 j_1 \left(\sqrt{\frac{6}{5}}\zeta r \right) + b_1 y_1 \left(\sqrt{\frac{6}{5}}\zeta r \right) \right] \cos\theta, \tag{116}$$

where

$$B = -1 - \frac{5}{6\zeta} i \left[a_1 j_1 \left(\sqrt{\frac{6}{5}}\zeta \right) + b_1 y_1 \left(\sqrt{\frac{6}{5}}\zeta \right) \right], \tag{117a}$$

$$c = \frac{5}{3} \left[a_0 j_0 \left(\sqrt{\frac{6}{5}}\zeta \right) + b_0 y_0 \left(\sqrt{\frac{6}{5}}\zeta \right) \right]. \tag{117b}$$

The continuity equation then gives the velocity field,

$$\begin{aligned} \bar{v}_{H|i}^{(0)} = -\frac{5i}{6\zeta} \Bigg\{ \sqrt{\frac{6}{5}}\zeta \Bigg[a_0 j_0' \left(\sqrt{\frac{6}{5}}\zeta r \right) + b_0 y_0' \left(\sqrt{\frac{6}{5}}\zeta r \right) + \left(a_1 j_1' \left(\sqrt{\frac{6}{5}}\zeta r \right) + b_1 y_1' \left(\sqrt{\frac{6}{5}}\zeta r \right) \right) \cos\theta \Bigg] \hat{\boldsymbol{r}} - \\ \left[a_1 j_1 \left(\sqrt{\frac{6}{5}}\zeta r \right) + b_1 y_1 \left(\sqrt{\frac{6}{5}}\zeta r \right) \right] \frac{\sin\theta}{r} \hat{\boldsymbol{\theta}} \Bigg\}, \end{aligned} \tag{118}$$

where $'$ indicates the derivative.

Matching the angular and radial components of the velocity between the Hilbert and viscous regions, respectively, requires

$$a_0 j_0' \left(\sqrt{\frac{6}{5}}\zeta \right) + b_0 y_0' \left(\sqrt{\frac{6}{5}}\zeta \right) = 0, \tag{119a}$$

$$a_1 j_1' \left(\sqrt{\frac{6}{5}}\zeta \right) + b_1 y_1' \left(\sqrt{\frac{6}{5}}\zeta \right) = \sqrt{\frac{6}{5}} i, \tag{119b}$$

which is to be imposed together with the Sommerfeld radiation condition [50] (restricting the solution to outgoing waves),

$$\lim_{r\to\infty} r \left(\frac{\partial}{\partial r} - i\sqrt{\frac{6}{5}}\zeta \right) \sigma_H^{(0)} = 0. \tag{120}$$

Equation (120) gives

$$b_0 = -i a_0, \qquad b_1 = i a_1, \tag{121}$$

which together with Eq. (119) determine the remaining unknown coefficients,

$$a_0 = b_0 = 0, \qquad a_1 = -i b_1 = \frac{i}{j_1'\left(\sqrt{\frac{6}{5}}\zeta\right) + i y_1'\left(\sqrt{\frac{6}{5}}\zeta\right)} \sqrt{\frac{6}{5}}. \tag{122}$$

2. First-order solution ($n = 1$)

The Knudsen corrections follow directly from the leading-order solution in the viscous region using the formulas in Table III; they are not produced here.

Turning to the viscous region, the corresponding boundary conditions are

$$\tau_{V0}^{(1)} = W_0\sqrt{\zeta}(-1+i)\left(\tau_b - \frac{2}{5}P_V^{(0)}\right), \qquad \bar{v}_{V0|i}^{(1)}t_i^1 = Z_0 B\sqrt{\zeta}(-1+i)\sin\theta, \tag{123}$$

with viscous normal velocity again satisfying the no-penetration condition. Integrating the pressure equation gives

$$P_V^{(1)} = 2i\zeta y\cos\theta + d(\theta), \tag{124}$$

where the function, $d(\theta)$ is to be determined by matching with the Hilbert region (below).

Integrating the momentum equation for the normal velocity gives

$$\bar{v}_{V|i}^{(1)}n_i = i\zeta\left(\frac{3}{5}P_V^{(0)}y - \frac{1}{\sqrt{\zeta}(-1+i)}\left(\tau_b - \frac{2}{5}P_V^{(0)}\right)(e^{\sqrt{\zeta}(-1+i)y}-1)\right) - 2B\left(\frac{e^{\sqrt{\zeta}(-1+i)y}-1}{\sqrt{\zeta}(-1+i)} - y\right)\cos\theta, \tag{125}$$

while solution to the temperature equation yields

$$\tau_V^{(1)} = -\left[\left(\tau_b - \frac{2}{5}P_V^{(0)}\right)y + C(\theta)\right]e^{\sqrt{\zeta}(-1+i)y} + \frac{4}{5}i\zeta y\cos\theta + \frac{2}{5}d(\theta), \tag{126a}$$

$$\sigma_V^{(1)} = \left[\left(\tau_b - \frac{2}{5}P_V^{(0)}\right)y + C(\theta)\right]e^{\sqrt{\zeta}(-1+i)y} + \frac{6}{5}i\zeta y\cos\theta + \frac{3}{5}d(\theta), \tag{126b}$$

where $C(\theta)$ is also to be evaluated and the temperature boundary condition requires

$$\frac{2}{5}d(\theta) - C(\theta) = W_0\sqrt{\zeta}(-1+i)\left(\tau_b - \frac{2}{5}P_V^{(0)}\right). \tag{127}$$

The tangential velocity follows similarly,

$$\bar{v}_{V|i}^{(1)}t_i^1 = e^{\sqrt{\zeta}(-1+i)y}\left(-\frac{d'(\theta)}{2i\zeta} + Z_0 B\sqrt{\zeta}(-1+i)\sin\theta\right) + By\sin\theta + \frac{d'(\theta)}{2i\zeta} - Bye^{\sqrt{\zeta}(-1+i)y}\sin\theta. \tag{128}$$

The Hilbert equations give

$$\sigma_H^{(1)} = E_0 j_0\left(\sqrt{\frac{6}{5}}\zeta r\right) + F_0 y_0\left(\sqrt{\frac{6}{5}}\zeta r\right) + \left[E_1 j_1\left(\sqrt{\frac{6}{5}}\zeta r\right) + F_1 y_1\left(\sqrt{\frac{6}{5}}\zeta r\right)\right]\cos\theta, \tag{129a}$$

$$P_H^{(1)} = \frac{5}{3}\sigma_H^{(1)}, \tag{129b}$$

$$\bar{v}_{H|i}^{(1)} = -\frac{5i}{6\zeta}\frac{\partial\sigma_H^{(1)}}{\partial x_i}, \tag{129c}$$

and the Sommerfeld radiation condition produces

$$E_0 + iF_0 = 0, \qquad iE_1 - F_1 = 0. \tag{130}$$

Finally, we apply the matching condition between the Hilbert and viscous regions,

$$\phi_V^{(1)} \sim \phi_{H0}^{(1)} + yn\frac{\partial\phi_{H0}^{(0)}}{\partial x_i}, \qquad y \to \infty, \tag{131}$$

which gives

$$d(\theta) = \frac{5}{3}\left\{E_0 j_0\left(\sqrt{\frac{6}{5}}\zeta\right) + F_0 y_0\left(\sqrt{\frac{6}{5}}\zeta\right) + \left[E_1 j_1\left(\sqrt{\frac{6}{5}}\zeta\right) + F_1 y_1\left(\sqrt{\frac{6}{5}}\zeta\right)\right]\cos\theta\right\}. \tag{132}$$

It can be shown that Eq. (132) ensures that the tangential velocities in the Hilbert and viscous regions match. Matching the normal velocities gives

$$\frac{i\sqrt{\zeta}}{-1+i}\left(\tau_b - \frac{2}{5}c\right) = -\frac{5i}{6\zeta}\sqrt{\frac{6}{5}}\zeta\left(E_0 j_0'\left(\sqrt{\frac{6}{5}}\zeta\right) + F_0 y_0'\left(\sqrt{\frac{6}{5}}\zeta\right)\right), \tag{133a}$$

$$\frac{i\sqrt{\zeta}}{-1+i}\left(-\frac{4}{5}i\zeta(1+B)\right) + \frac{2B}{\sqrt{\zeta}(-1+i)} = -\frac{5i}{6}\sqrt{\frac{6}{5}}\left(E_1 j_1'\left(\sqrt{\frac{6}{5}}\zeta\right) + F_1 y_1'\left(\sqrt{\frac{6}{5}}\zeta\right)\right), \tag{133b}$$

which together with Eq. (130) determines E_0, E_1, F_0 and F_1; the coefficients B and c are defined in Eq. (117).

3. Second-order solution ($n = 2$)

Because the leading-order Hilbert moments are nonzero, the density equation here is an inhomogeneous Helmholtz equation. Manipulations give

$$\frac{\partial^2 \sigma_H^{(2)}}{\partial {x_j}^2} + \frac{6}{5}\zeta^2\sigma_H^{(2)} = -\frac{36}{25}i\zeta^3\sigma_H^{(0)}. \tag{134}$$

Noting that $\sigma_H^{(0)}$ comprises of four terms then gives the general solution,

$$\begin{aligned}\sigma_H^{(2)} &= p_1(r) + p_2(r) + p_3(r,\theta) + p_4(r,\theta) + \\ &a_2 j_0\left(\sqrt{\frac{6}{5}}\zeta r\right) + b_2 y_0\left(\sqrt{\frac{6}{5}}\zeta r\right) + \cos\theta\left(a_3 j_1\left(\sqrt{\frac{6}{5}}\zeta r\right) + b_3 y_1\left(\sqrt{\frac{6}{5}}\zeta r\right)\right),\end{aligned} \tag{135}$$

where the coefficients, a_2, a_3, b_2, b_3, are to be determined, and

$$\begin{aligned}p_1(r) = \frac{36}{25}\sqrt{\frac{6}{5}}i\zeta^4 a_0\Bigg[&j_0\left(\sqrt{\frac{6}{5}}\zeta r\right)\int_1^r y_0\left(\sqrt{\frac{6}{5}}\zeta r'\right) j_0\left(\sqrt{\frac{6}{5}}\zeta r'\right) r'^2\,dr' \\ &-y_0\left(\sqrt{\frac{6}{5}}\zeta r\right)\int_1^r j_0^2\left(\sqrt{\frac{6}{5}}\zeta r'\right) r'^2\,dr'\Bigg],\end{aligned} \tag{136a}$$

$$\begin{aligned}p_2(r) = \frac{36}{25}\sqrt{\frac{6}{5}}i\zeta^4 b_0\Bigg[&j_0\left(\sqrt{\frac{6}{5}}\zeta r\right)\int_1^r y_0^2\left(\sqrt{\frac{6}{5}}\zeta r'\right) r'^2\,dr' \\ &-y_0\left(\sqrt{\frac{6}{5}}\zeta r\right)\int_1^r j_0\left(\sqrt{\frac{6}{5}}\zeta r'\right) y_0\left(\sqrt{\frac{6}{5}}\zeta r'\right) r'^2\,dr'\Bigg],\end{aligned} \tag{136b}$$

$$\begin{aligned}p_3(r,\theta) = \frac{36}{25}\sqrt{\frac{6}{5}}i\zeta^4 a_1\cos\theta\Bigg[&j_1\left(\sqrt{\frac{6}{5}}\zeta r\right)\int_1^r y_1\left(\sqrt{\frac{6}{5}}\zeta r'\right) j_1\left(\sqrt{\frac{6}{5}}\zeta r'\right) r'^2\,dr' \\ &-y_1\left(\sqrt{\frac{6}{5}}\zeta r\right)\int_1^r j_1^2\left(\sqrt{\frac{6}{5}}\zeta r'\right) r'^2\,dr'\Bigg],\end{aligned} \tag{136c}$$

$$\begin{aligned}p_4(r,\theta) = \frac{36}{25}\sqrt{\frac{6}{5}}i\zeta^4 b_1\cos\theta\Bigg[&j_1\left(\sqrt{\frac{6}{5}}\zeta r\right)\int_1^r y_1^2\left(\sqrt{\frac{6}{5}}\zeta r'\right) r'^2\,dr' \\ &-y_1\left(\sqrt{\frac{6}{5}}\zeta r\right)\int_1^r j_1\left(\sqrt{\frac{6}{5}}\zeta r'\right) y_1\left(\sqrt{\frac{6}{5}}\zeta r'\right) r'^2\,dr'\Bigg],\end{aligned} \tag{136d}$$

from which the other moments directly follow using

$$\bar{v}^{(2)}_{H|j} = \frac{5}{6i\zeta}\frac{\partial \sigma^{(2)}_H}{\partial x_j} - \frac{\partial \sigma^{(0)}_H}{\partial x_j}, \qquad P^{(2)}_H = \frac{5}{3}\sigma^{(2)}_H - \frac{2}{3}i\zeta\sigma^{(0)}_H, \qquad \tau^{(2)}_H = \frac{2}{3}\sigma^{(2)}_H - \frac{2}{3}i\zeta\sigma^{(0)}_H. \tag{137}$$

The Sommerfeld radiation condition gives

$$b_2 = \frac{1}{5}\left(5a_2 i + 3a_0\zeta e^{2i\sqrt{\frac{6}{5}}\zeta}\right), \qquad b_3 = ia_3 - \frac{1}{5}a_1 e^{2i\sqrt{\frac{6}{5}}\zeta}(\sqrt{30} - 3i\zeta), \tag{138}$$

with an additional two constraints determined in a similar manner to that used for the first-order solution; details are omitted due to their complexity. This system of 4 linear equations specifies the coefficients, a_2, a_3, b_2 and b_3.

4. Comparison to numerical solutions of the Boltzmann-BGK equation

These asymptotic solutions are now validated against accurate numerical solutions. We also make a comparison to a solution derived from the compressible linearized Navier Stokes equation with the slip and temperature jump condition. Here, we choose $\tau_b = 0$ (sphere is held at the ambient temperature) and an acoustic wavenumber of $\zeta = 1$. The exact numerical solution is computationally expensive and we restrict our comparison to the moderate Knudsen number of $k = 0.025$ (computational expense increases with reduced k). For simplicity, we again only report results for the velocity field since our primary aim is to assess the validity of the asymptotic theory.

Numerical solution: As in Section IV B, the method of Ref. [21] is used to obtain accurate numerical solutions; the specific case considered here is also detailed in Ref. [54]. Because the flow is axisymmetric, it follows that the distribution function is independent of the ϕ azimuthal coordinate. Spherical symmetry also specifies the functional dependence on the θ polar coordinate [55]. Therefore, the problem reduces to a one-dimensional boundary value problem in terms of the r radial coordinate in the spatial domain, $r \in [1, R)$ as $R \to \infty$. As per Ref. [54], a spatially varying second-order upwind finite difference scheme is employed, with finer discretization near the surface of the sphere. The (true) unbounded spatial domain is simulated by using successively larger values of R until the solution converges. As in Section IV B, polynomials with compact support are used to represent the solution in three-dimensional particle velocity space. The location of the expected discontinuities in particle velocity space is a function of the spatial coordinate. The general approach to this type of problem is discussed in Ref. [21], and again application to this problem is detailed in Ref. [54]. The numerical solution reported here is obtained by systematically doubling the number of spatial points, doubling the value of R, and increasing the order of the basis functions by one, until the relative change in all transport variables is less than 1%. Numerical results are given for 96,000 spatial points with polynomials of order 8 and $R = 60$.

Figures 7 and 8 give results for the velocity field, normal and tangential to the surface along $\theta = 0$ and $\pi/2$, respectively. Comparison to the present asymptotic theory correct to $O(1)$ and $O(\epsilon)$ is provided in Fig. 7. This shows that a significant improvement is afforded through inclusion of the $O(\epsilon)$ correction, while both solutions give reasonable agreement with the exact numerical solution. These asymptotic theories are similarly accurate in the outer part of the Hilbert region, i.e., $r \gg 1$, due to the decaying nature of the solution, with the oscillations corresponding to wave motion with an acoustic wavenumber of $\zeta = 1$. In contrast, significant discrepancies exist closer to the surface. The $O(1)$ theory intrinsically includes the no-slip condition, see Eq. (112a), which is evident in Fig. 7. Finite slip and temperature jump emerges at $O(\epsilon)$ with the asymptotic solution agreeing reasonably well with the exact numerical solution.

Including the $O(\epsilon^2)$ correction in the present asymptotic theory strongly improves agreement with the exact numerical solution; see Fig. 8. The intricate structure and variations in the exact solution are well captured by the asymptotic theory, while some discrepancies remain. The most significant discrepancy occurs in the imaginary part of the normal velocity in the (matching) overlap region between the viscous and Hilbert regions. This is not surprising given $k = 0.025$ is not very small and the composite solution in Eq. (57) is used in this comparison. Indeed, comparison at a larger value of k accentuates these differences, as expected (data not shown). Further comparisons using smaller Knudsen numbers are inhibited by numerical difficulties arising due to the higher dimensionality of this problem. The solution obtained using the NSF equations with the slip and temperature jump conditions is also shown in Fig. 8, and is also found to agree well with the exact numerical solution. Some discrepancies are also visible in this NSF solution, but are not dissimilar in strength relative to those of the asymptotic theory correct to $O(\epsilon^2)$.

Unlike Applications 1 and 2, which are bounded flows in the wall-normal directions, resonances are not possible here because the flow is unbounded—interference between forward and backward travelling waves is not possible.

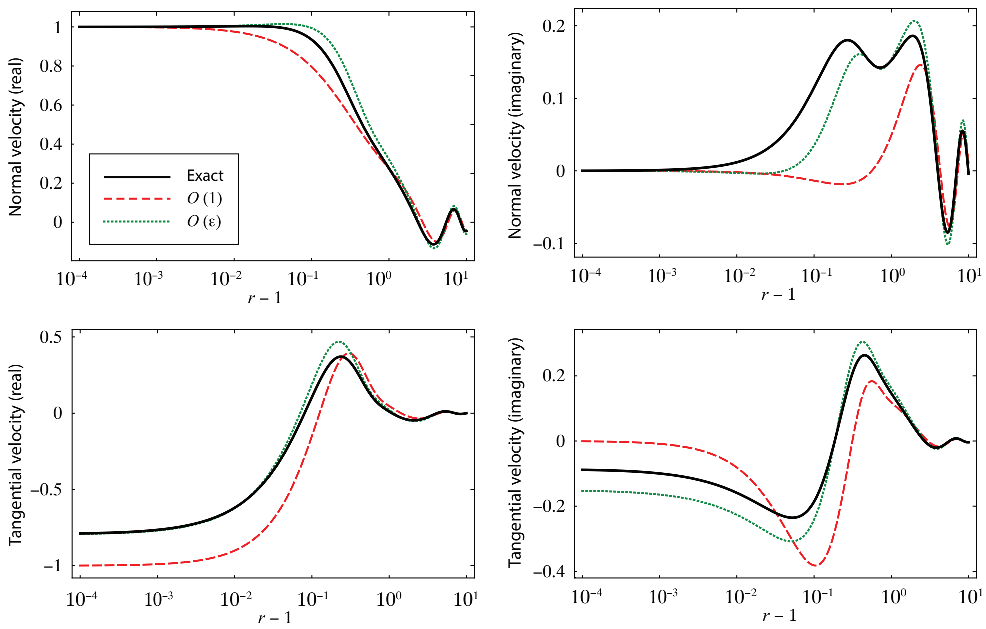

FIG. 7: Comparison of normal and tangential velocities in gas versus radial position, r, evaluated at $\theta = 0$ and $\pi/2$, respectively. Data shown for $k = 0.025$ and $\zeta = 1$, as determined by the exact numerical solution (solid line – black), asymptotic theory correct to $O(1)$ (dashed line – red) and asymptotic theory correct to $O(\epsilon)$ (dotted line – green). As an approximate guide, Knudsen region ($r - 1 \lesssim 0.025$); viscous region ($0.025 \lesssim r - 1 \lesssim 0.16$); Hilbert region ($r - 1 \gtrsim 0.16$).

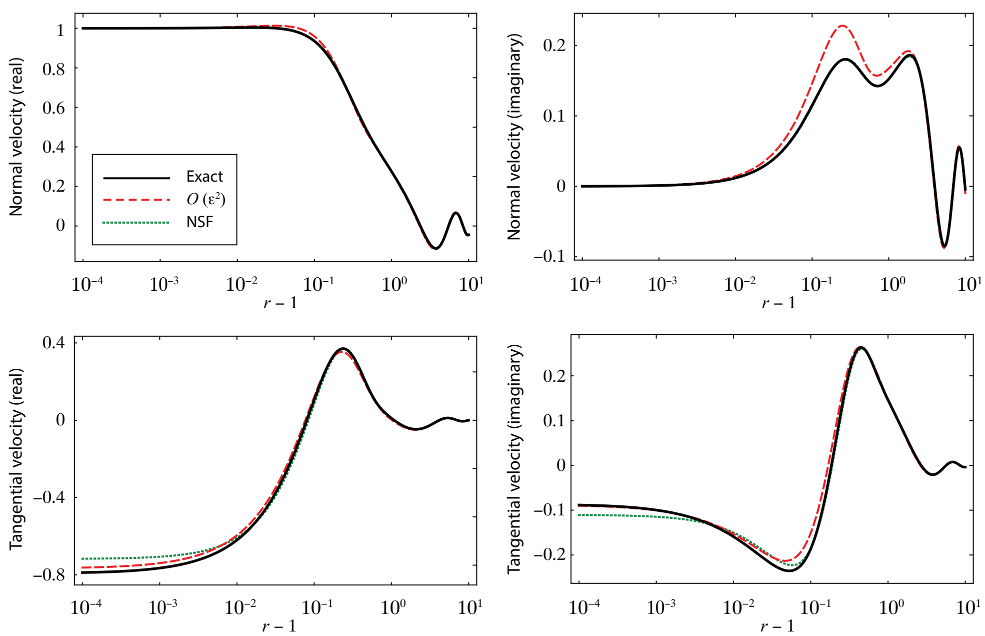

FIG. 8: As for Fig. 7, but with exact numerical solution (solid line – black), asymptotic theory correct to $O(\epsilon^2)$ (dashed line – red) and NSF equation with slip and temperature jump condition (NSF) (dotted line – green).

V. SLIP BOUNDARY CONDITION FOR TANGENTIAL VELOCITY

Previous asymptotic analyses of the Boltzmann-BGK equation in the limit of small k have recovered the following leading-order expression for the tangential slip velocity,

$$(\bar{v}_i - V_i)t_i^1 = k\left(-Z_0 n_i t_j^1\left[\frac{\partial \bar{v}_i}{\partial x_j} + \frac{\partial \bar{v}_j}{\partial x_i}\right] - G_3 t_i^1 \frac{\partial \tau}{\partial x_i}\right) + o(k), \tag{139}$$

which holds for both steady and unsteady (quasi-incompressible, long wavelength) flows [34, 35, 47]; Aoki *et al.* [41] also showed that it holds for the compressible Navier Stokes equation, by using a Chapman-Enskog formulation. We now examine the validity of this slip formula for acoustic flows (studied here) by comparison to the corresponding asymptotic formula in Table III, also correct to $O(k)$.

To begin, we note that the corresponding slip condition in the present acoustic problem is applied to the inner part of the viscous region; rather than the Hilbert region for quasi-incompressible flows, as required for use of Eq. (139). Indeed, the Hilbert region implicitly contains the viscous region for quasi-incompressible flows. To compare these slip formulas, the outer Cartesian variables in Eq. (139) are rewritten in terms of the rescaled coordinates of the viscous region, i.e.,

$$\frac{\partial}{\partial x_i} = \frac{n_i}{\epsilon}\frac{\partial}{\partial y} + \left(\frac{\partial \chi_1}{\partial x_i}\right)_0 \frac{\partial}{\partial \chi_1} + \left(\frac{\partial \chi_2}{\partial x_i}\right)_0 \frac{\partial}{\partial \chi_2}. \tag{140}$$

Substituting Eq. (140) into Eq. (139) then gives the equivalent expression,

$$(\bar{v}_i - V_i)t_i^1 = -\epsilon Z_0 \frac{\partial \bar{v}_i}{\partial y} - \epsilon^2 Z_0 n_i t_j^1 \left(\frac{\partial \chi_1}{\partial x_j}\right)_0 \frac{\partial \bar{v}_i}{\partial \chi_1} - \epsilon^2 G_3 t_i^1 t_i^1 \frac{\partial \tau}{\partial \chi_1} + o(\epsilon^2), \tag{141}$$

which can be compared directly to the corresponding acoustic slip formula in Table III, which we now present.

Combining the asymptotic slip formulas in Table III for the tangential slip velocity, at $O(\epsilon)$ and $O(\epsilon^2)$, and using the identity, $G_2 = G_4 = Z_0$, gives

$$(\bar{v}_i - V_i)t_i^1 = -\epsilon Z_0 \frac{\partial \bar{v}_i}{\partial y} - \epsilon^2 Z_0 n_i t_j^1 \left(\frac{\partial \chi_1}{\partial x_j}\right)_0 \frac{\partial \bar{v}_i}{\partial \chi_1} - \epsilon^2 G_3 t_i^1 t_i^1 \frac{\partial \tau}{\partial \chi_1} + \epsilon^2 G_1 \frac{\partial^2 \bar{v}_i t_i^1}{\partial y^2} + o(\epsilon^2), \tag{142}$$

which is strikingly similar to Eq. (141). The only difference is the existence of a shear stress (second-order spatial derivative) term in Eq. (142). But this term coincides with the second derivative term in the second-order steady boundary condition, Eq. (3). This is evident upon replacement of the outer coordinate used in Eq. (142) with the rescaled normal coordinate of the viscous region. Indeed, the coefficient -0.7667 in Eq. (3) agrees with our calculated value of $-G_1 = 0.766322$, correct to three decimal places; see Eq. (B2). This shows that the present formulation includes effects found in the widely studied steady flow problem correct to $O(k^2)$ [22, 38].

VI. CONCLUSIONS

We have presented a rigorous asymptotic analysis of the Boltzmann-BGK equation for slightly rarefied gas flows, i.e., small Knudsen number, where the acoustic wavelength is comparable to the geometric length scale of the flow domain. Unlike previous long-wavelength (quasi-incompressible) flows [34, 35, 47], these acoustic flows confine the effects of viscosity to a thin boundary layer near the solid surface. This leads to the appearance of three length scales: the aforementioned geometric length scale, the viscous penetration depth, and the mean free path of the gas, in order of asymptotically decreasing size. Transport equations and boundary conditions for these regions were thus derived using a three-way matched asymptotic expansion.

The validity of the presented asymptotic theory was assessed by its application to three canonical problems: (i) oscillatory (time-dependent) heating of a gas confined between two walls, (ii) oscillatory thermal creep between two walls, and (iii) the rectilinear oscillation of a solid sphere in a quiescent gas. Benchmark numerical results for the first and third applications were computed using the recent variational formulation of Ref. [21]. Excellent agreement between numerical results and the present asymptotic theory was found. The second application was compared to the long-wavelength asymptotic solution of Ref. [34], where overlap between their respective regimes of validity was observed, as expected. Demonstration of these applications highlights the utility of the present asymptotic theory in deriving analytical solutions for rarefied gas flows of practical interest, that would otherwise require sophisticated numerical methods.

ACKNOWLEDGEMENTS

The authors gratefully acknowledge support from the Australian Research Council Centre of Excellence in Exciton Science (Grant No. CE170100026) and the Australian Research Council Grants Scheme. D.R.L. also acknowledges support from the U.S. Department of Energy, Office of Science, Office of Advanced Scientific Computing Research, Applied Mathematics Program under Contract No. DE-AC02-05CH11231.

Appendix A: Integral equations for the Knudsen region

1. First-order integral equations ($n = 1$)

The integral equations defining the Knudsen correction at $O(\epsilon)$ are

$$\sigma_b^{(1)} - \sigma_{V0}^{(1)} = -\frac{1}{2}(\tau_b^{(1)} - \tau_{V0}^{(1)}) + 2\Xi(\sigma_K^{(1)}, \tau_K^{(1)}), \tag{A1a}$$

$$\sqrt{\pi}\bar{v}_{K|i}^{(1)} t_i^1 = (V_i^{(1)} - \bar{v}_{V0|i}^{(1)}) t_i^1 J_0(\eta) + \int_0^\infty \bar{v}_{K|i}^{(1)} t_i^1 J_{-1}(|\eta - \eta_0|)\, d\eta_0 + \frac{\partial \bar{v}_{V0|i}^{(0)} t_i^1}{\partial y} J_1(\eta), \tag{A1b}$$

$$\sqrt{\pi}\sigma_K^{(1)} = (\tau_b^{(1)} - \tau_{V0}^{(1)})\,(J_2(\eta) - J_0(\eta)) + 2\Xi(\sigma_K^{(1)}, \tau_K^{(1)}) J_0(\eta) + L_1(\sigma_K^{(1)}, \tau_K^{(1)}) + \frac{\partial \tau_{V0}^{(0)}}{\partial y}\left(J_3(\eta) - \frac{3}{2}J_1(\eta)\right), \tag{A1c}$$

$$\begin{aligned}\frac{3}{2}\sqrt{\pi}\tau_K^{(1)} = (\tau_b^{(1)} - \tau_{V0}^{(1)})\left(J_4(\eta) - \frac{3}{2}J_2(\eta) + \frac{3}{2}J_0(\eta)\right) + \Xi(\sigma_K^{(1)}, \tau_K^{(1)})(2J_2(\eta) - J_0(\eta)) + L_2(\sigma_K^{(1)}, \tau_K^{(1)}) +\\ \frac{\partial \tau_{V0}^{(0)}}{\partial y}\left(\frac{7}{4}J_1(\eta) - 2J_3(\eta) + J_5(\eta)\right),\end{aligned} \tag{A1d}$$

$$\begin{aligned}\sqrt{\pi}P_{K|ij}^{(1)} t_i^m t_j^m = \int_0^\infty \sigma_K^{(1)} J_{-1}(|\eta - \eta_0|) + \tau_K^{(1)}\left(J_1(|\eta - \eta_0|) + \frac{1}{2}J_{-1}(|\eta - \eta_0|)\right) d\eta_0 +\\ \left(2\Xi(\sigma_K^{(1)}, \tau_K^{(1)}) J_0(\eta) + \left(\tau_b^{(1)} - \tau_{V0}^{(1)}\right) J_2(\eta) + \frac{\partial \tau_{V0}^{(0)}}{\partial y}\left(J_3(\eta) - \frac{1}{2}J_1(\eta)\right)\right), \qquad m \in \{1, 2\},\end{aligned} \tag{A1e}$$

which uses the following operators,-

$$\Xi(f(x), g(x)) = \int_0^\infty f(x) J_0(x) + g(x)\left(J_2(x) - \frac{1}{2}J_0(x)\right) dx, \tag{A2a}$$

$$L_1(f(\eta), g(\eta)) = \int_0^\infty f(\eta_0) J_{-1}(|\eta - \eta_0|) + g(\eta_0)\left(J_1(|\eta - \eta_0|) - \frac{1}{2}J_{-1}(|\eta - \eta_0|)\right) d\eta_0, \tag{A2b}$$

$$\begin{aligned}L_2(f(\eta), g(\eta)) = \int_0^\infty f(\eta_0)\left(J_1(|\eta - \eta_0|) - \frac{1}{2}J_{-1}(|\eta - \eta_0|)\right) +\\ g(\eta_0)\left(J_3(|\eta - \eta_0|) - J_1(|\eta - \eta_0|) + \frac{5}{4}J_{-1}(|\eta - \eta_0|)\right) d\eta_0.\end{aligned} \tag{A2c}$$

The Abramowitz functions, $J_n(x)$, are [56]

$$J_n(x) = \int_0^\infty t^n e^{-t^2 - \frac{x}{t}}\, dt, \qquad x \geq 0. \tag{A3}$$

The above integral equations are solved using a refined moment method [47], in which each moment is written as linear combinations of the inhomogeneities in each equation. This gives the slip conditions in Table III, where each function of η is expressed as a linear combination of Abramowitz functions,

$$Y_1(\eta) = \sum_{s=0}^{n} y_{1,s} J_s(\eta), \qquad Y_2(\eta) = \sum_{s=0}^{n} y_{2,s} J_s(\eta), \tag{A4a}$$

$$X_1(\eta) = \sum_{s=0}^{n} x_{1,s} J_s(\eta), \qquad X_2(\eta) = \sum_{s=0}^{n} x_{2,s} J_s(\eta), \tag{A4b}$$

where $y_{1,s}, \rho_s, x_{1,s}, x_{2,s}$ are constants, and n is a positive integer that is systematically increased to convergence. This gives $3n + 5$ parameters in total.

Taking n moments of Eqs. (A1) gives $3n$ equations. Then, using the asymptotic expression as $\eta \to 0^+$,

$$J_0(\eta) \sim \frac{\sqrt{\pi}}{2} + \eta \log(\eta), \tag{A5}$$

$$\int_0^\infty f(\eta_0) J_{-1}(|\eta - \eta_0|)\, d\eta_0 \sim -f(0)\eta \log(\eta), \tag{A6}$$

allows 3 more equations to be generated by evaluating Eqs. (A1) at $\eta = 0$, with an additional 3 equations obtained by comparing the $\eta \log(\eta)$ asymptotic dependencies on both sides of Eqs. (A1). One of the equations can be shown to be redundant, leading to $3n+5$ linear equations in $3n+5$ parameters. Numerical results of this procedure are given in Appendix B.

2. Second-order integral equations ($n = 2$)

The same procedure results in the following integral equations,

$$\begin{aligned}
\sqrt{\pi}\sigma_K^{(2)} = {} & 2\Xi\left(\sigma_K^{(2)}, \tau_K^{(2)}\right) J_0(\eta) + \left(\tau_b^{(2)} - \tau_{V0}^{(2)}\right)(J_2(\eta) - J_0(\eta)) + \\
& \int_0^\infty \sigma_K^{(2)} J_{-1}(|\eta - \eta_0|) + \tau_K^{(2)}\left(J_1(|\eta-\eta_0|) - \frac{1}{2}J_{-1}(|\eta-\eta_0|)\right) d\eta_0 + \\
& \frac{\partial \tau_{V0}^{(1)}}{\partial y}\left(J_3(\eta) - \frac{3}{2}J_1(\eta)\right) - i\zeta\left(\sigma_{V0}^{(0)}\left(\frac{8}{5}J_0(\eta) - \frac{16}{5}J_2(\eta) + \frac{4}{5}J_4(\eta)\right) + \right. \\
& \left. \tau_{V0}^{(0)}\left(-\frac{6}{5}J_4(\eta) + \frac{14}{5}J_2(\eta) - \frac{2}{5}J_0(\eta)\right)\right) + \left(\frac{\partial\chi_1}{\partial x_j}\frac{\partial}{\partial\chi_1} + \frac{\partial\chi_2}{\partial x_j}\frac{\partial}{\partial\chi_2}\right)(\bar{v}_{V0|j}^{(0)})(2J_0(\eta) - 2J_2(\eta)),
\end{aligned} \tag{A7a}$$

$$\begin{aligned}
\sqrt{\pi}\bar{v}_{K|i}^{(2)} t_i^1 = {} & (V_i^{(2)} - \bar{v}_{V0|i}^{(2)}) t_i^1 J_0(\eta) + \int_0^\infty \bar{v}_{K|i}^{(2)} t_i^1 J_{-1}(|\eta - \eta_0|)\, d\eta_0 + \frac{\partial \bar{v}_{V0|i}^{(1)} t_i^1}{\partial y} J_1(\eta) + \\
& \frac{\partial^2 \bar{v}_{V0|i}^{(0)} t_i^1}{\partial y^2}\left(\frac{1}{2}J_0(\eta) - J_2(\eta)\right) + n_k t_j^1 \frac{\partial\chi_1}{\partial x_j}\frac{\partial \bar{v}_{V0|k}^{(0)}}{\partial\chi_1} J_1(\eta) + \frac{1}{2}t_i^1 \frac{\partial\chi_1}{\partial x_i}\frac{\partial\tau_{V0}^{(0)}}{\partial\chi_1}\left(J_2(\eta) - \frac{1}{2}J_0(\eta)\right),
\end{aligned} \tag{A7b}$$

$$\begin{aligned}
\frac{3}{2}\sqrt{\pi}\tau_K^{(2)} = {} & \Xi\left(\sigma_K^{(2)}, \tau_K^{(2)}\right)(2J_2(\eta) - J_0(\eta)) + (\tau_b^{(2)} - \tau_{V0}^{(2)})\left(J_4(\eta) - \frac{3}{2}J_2(\eta) + \frac{3}{2}J_0(\eta)\right) + \\
& L_2(\sigma_K^{(2)}, \tau_K^{(2)}) + \frac{\partial\tau_{V0}^{(1)}}{\partial y}\left(\frac{7}{4}J_1(\eta) - 2J_3(\eta) + J_5(\eta)\right) - i\zeta\left(\sigma_{V0}^{(0)}\left(\frac{4}{5}J_6(\eta) - \frac{18}{5}J_4(\eta) + 4J_2(\eta) - \frac{4}{5}J_0(\eta)\right) + \right. \\
& \left. \tau_{V0}^{(0)}\left(\frac{6}{5}J_0(\eta) - 3J_2(\eta) + \frac{17}{5}J_4(\eta) - \frac{6}{5}J_6(\eta)\right)\right) + \left(\frac{\partial\chi_1}{\partial x_j}\frac{\partial}{\partial\chi_1} + \frac{\partial\chi_2}{\partial x_j}\frac{\partial}{\partial\chi_2}\right)(\bar{v}_{V0|j}^{(0)})(-2J_4(\eta) + 3J_2(\eta)),
\end{aligned} \tag{A7c}$$

$$\begin{aligned}
\sqrt{\pi}P_{K|ij}^{(2)} t_i^m t_j^m = {} & \int_0^\infty \sigma_K^{(2)} J_{-1}(|\eta-\eta_0|) + \tau_K^{(2)}\left(J_1(|\eta-\eta_0|) + \frac{1}{2}J_{-1}(|\eta-\eta_0|)\right) d\eta_0 + \\
& \left(2\Xi(\sigma_K^{(2)}, \tau_K^{(2)}) J_0(\eta) + \left(\tau_b^{(2)} - \tau_{V0}^{(2)}\right) J_2(\eta) + 2\frac{\partial \bar{v}_{V0|i}^{(1)} n_i}{\partial y} J_2(\eta) + \frac{\partial\tau_{V0}^{(1)}}{\partial y}\left(J_3(\eta) - \frac{1}{2}J_1(\eta)\right)\right) - \\
& i\zeta\left(2\sigma_{V0}^{(0)} J_0(\eta) + \tau_{V0}^{(0)} J_2(\eta)\right) - \frac{\partial^2\tau_{V0}^{(0)}}{\partial y^2}\left(J_4(\eta) - \frac{1}{2}J_2(\eta) - \frac{1}{2}J_0(\eta)\right) + \\
& \left(4t_i^m t_j^m \frac{\partial\chi_1}{\partial x_i}\frac{\partial\bar{v}_{V0|j}^{(0)}}{\partial\chi_1} + 2t_i^{3-m} t_j^{3-m}\frac{\partial\chi_2}{\partial x_i}\frac{\partial\bar{v}_{V0|j}^{(0)}}{\partial\chi_2}\right) J_0(\eta), \qquad m \in \{1, 2\}.
\end{aligned} \tag{A7d}$$

The solution procedure is identical to that used for first-order equations above.

The Abramowitz functions, $J_s(\eta)$, all decay exponentially with η. Expressing each of the Knudsen corrections as a sum of Abramowitz functions, as performed in the refined moment method above, is consistent with the constraint that the Knudsen corrections decay faster than any inverse power of η.

Appendix B: Slip coefficients

In this Appendix, we give numerical coefficients for the first-order and second-order slip conditions specified in Table III.

1. First-order slip coefficients ($n = 1$)

The first-order slip conditions in Table III use the expansions in Eqs. (A4) whose coefficients are given in Table IV, and

$$Z_0 = 1.01619, \qquad W_0 = 1.30271. \tag{B1}$$

These numerical coefficients are converged to the number of significant figures shown (n is increased systematically to $n = 7$).

TABLE IV: First-order slip formula coefficients for Table III.

s	$y_{1,s}$	$y_{2,s}$	$x_{1,s}$	$x_{2,s}$
0	−0.398944	0.199472	0.464527	−0.475877
1	1.04374	−0.462149	−1.38268	1.03227
2	−3.37502	1.17618	2.23484	−0.699085
3	6.04351	−1.62725	3.33904	−7.00658
4	−6.21114	1.14194	−13.3644	17.7204
5	3.42892	−0.717878	14.3498	−17.1407
6	−0.973953	0.206404	−6.43631	7.33731
7	0.104732	−0.0224174	1.06521	−1.18676

The slip coefficients agree with Refs. [32, 34, 47, 49] where $Z_0 = -k_0, W_0 = d_1$. Using the notation of [47], $x_{1,s} = a_s, x_{2,s} = b_s$. Similar coefficients for other collision models may also be found in the above literature.

2. Second-order slip coefficients ($n = 2$)

The second-order slip conditions in Table III use

$$\begin{aligned} &A_1 = -0.701586, \qquad A_2 = 1.71307, \qquad A_3 = 1.30271, \qquad A_4 = -0.660690, \\ &G_1 = -0.766322, \qquad G_2 = 1.01619, \qquad G_3 = 0.383161, \qquad G_4 = 1.01619, \end{aligned} \tag{B2}$$

together with the following expansions,

$$\begin{gathered} B_p(\eta) = \sum_{s=0}^{n} b_{p,s} J_s(\eta), \quad p = 1,2,3,4, \qquad C_q(\eta) = \sum_{s=0}^{n} c_{q,s} J_s(\eta), \quad q = 1,2,3,4, \\ M_d(\eta) = \sum_{s=0}^{n} m_{d,s} J_s(\eta), \quad d = 1,2,...,8, \end{gathered} \tag{B3}$$

whose coefficients are given in Tables V – VII. It is noted that $A_3 = W_0, G_2 = G_4 = Z_0$ and $m_{2,s} = m_{4,s} = m_{8,s} = y_{1,s}, c_{3,s} = m_{5,s} = x_{2,s}, b_{3,s} = x_{1,s}, m_{1,s} = m_{7,s}$.

TABLE V: Second-order slip formula coefficients for Table III; Part 1.

s	$b_{1,s}$	$b_{2,s}$	$b_{3,s}$	$b_{4,s}$	$c_{1,s}$	$c_{2,s}$
0	−0.807885	0.514976	0.464527	0.696851	0.330651	−0.725157
1	0.350937	0.423607	−1.382680	−0.950013	0.560246	0.861140
2	9.694015	−19.37118	2.234843	4.830153	−15.07515	23.30687
3	−52.43104	89.83990	3.339041	−11.19334	66.024046	102.9827
4	97.13291	160.6297	−13.36439	14.93035	−114.8504	179.451043
5	−82.78990	134.7080	14.34987	−10.52311	94.573433	−148.3773
6	32.84557	−52.99919	−6.436309	3.730840	−36.71110	57.83930
7	−4.950295	7.976728	1.065214	−0.551286	5.466471	−8.671018

TABLE VI: Second-order slip formula coefficients for Table III; Part 2.

s	$c_{3,s}$	$c_{4,s}$	$m_{1,s}$	$m_{2,s}$	$m_{3,s}$	$m_{4,s}$
0	−0.475877	0.229181	0.405403	−0.398944	−0.202702	−0.398944
1	1.032274	0.020771	−0.710548	1.043738	0.355274	1.043738
2	−0.699085	0.694151	3.178705	−3.375020	−1.589352	−3.375020
3	−7.006582	3.946670	−6.524735	6.043511	3.262367	6.043511
4	17.720385	−7.175464	7.931401	−6.211141	−3.965701	−6.211141
5	−17.140687	6.517195	−5.034212	3.428925	2.517106	3.428925
6	7.337307	−2.772651	1.627366	−0.973953	−0.813683	−0.973953
7	−1.186757	0.471311	−0.181370	0.104732	0.090685	0.104732

TABLE VII: Second-order slip formula coefficients for Table III; Part 3.

s	$m_{5,s}$	$m_{6,s}$	$m_{7,s}$	$m_{8,s}$
0	−0.475877	0.229181	0.405403	−0.398944
1	1.032274	0.020771	−0.710548	1.043738
2	−0.699085	0.694151	3.178705	−3.375020
3	−7.006582	3.946670	−6.524735	6.043511
4	17.720385	−7.175464	7.931401	−6.211141
5	−17.140687	6.517195	−5.034212	3.428925
6	7.337307	−2.772651	1.627366	−0.9739533
7	−1.186757	0.471311	−0.181370	0.104732

Appendix C: Transport equations in the viscous region in terms of principal curvature

In this Appendix, we express the governing equations for the viscous region in Table II in terms of the principal surface curvature defined in Eq. (55).

1. Leading-order transport equations ($n = 0$)

$$\frac{\partial \bar{v}^{(0)}_{V|i} n_i}{\partial y} = 0, \tag{C1a}$$

$$\frac{\partial P^{(0)}_V}{\partial y} = 0, \tag{C1b}$$

$$\frac{\partial^2 \bar{v}^{(0)}_{V|i} t^q_i}{\partial y^2} + 2i\zeta \bar{v}^{(0)}_{V|i} t^q_i = \frac{1}{h_q}\frac{\partial P^{(0)}_V}{\partial \chi_q} - 2\zeta a_{i,0} t^q_i, \tag{C1c}$$

$$\frac{\partial^2 \tau^{(0)}_V}{\partial y^2} + 2i\zeta \tau^{(0)}_V = \frac{4}{5} i\zeta P^{(0)}_V, \tag{C1d}$$

where $a_{i,0} = a_i|_{y=0}$.

2. First-order transport equations ($n = 1$)

$$\frac{\partial \bar{v}^{(1)}_{V|i} n_i}{\partial y} = i\zeta\sigma^{(0)}_V - (\kappa_1 + \kappa_2)\bar{v}^{(0)}_{V|j} n_j - g_2 \bar{v}^{(0)}_{V|j} t^1_j - \frac{1}{h_1}\frac{\partial \bar{v}^{(0)}_{V|j} t^1_j}{\partial \chi_1} + g_1 \bar{v}^{(0)}_{V|j} t^2_j - \frac{1}{h_2}\frac{\partial \bar{v}^{(0)}_{V|j} t^2_j}{\partial \chi_2}, \tag{C2a}$$

$$\frac{\partial P^{(1)}_V}{\partial y} = 2i\zeta \bar{v}^{(0)}_{V|i} n_i + 2\zeta a_{i,0} n_i, \tag{C2b}$$

$$\frac{\partial^2 \bar{v}^{(1)}_{V|i} t^q_i}{\partial y^2} + 2i\zeta \bar{v}^{(1)}_{V|i} t^q_i = \frac{1}{h_q}\frac{\partial P^{(1)}_V}{\partial \chi_q} - \frac{\partial \bar{v}^{(0)}_{V|i} t^q_i}{\partial y}(\kappa_1 + \kappa_2) + \frac{y}{h_q}\frac{\partial P^{(0)}_V}{\partial \chi_q}, \tag{C2c}$$

$$\frac{\partial^2 \tau^{(1)}_V}{\partial y^2} + 2i\zeta \tau^{(1)}_V = \frac{4}{5} i\zeta P^{(1)}_V + \frac{\partial \sigma^{(0)}_V}{\partial y}\left(\kappa_1 + \kappa_2\right). \tag{C2d}$$

3. Second-order transport equations ($n = 2$)

$$\frac{\partial P_V^{(2)}}{\partial y} = 2i\zeta\bar{v}_{V|i}^{(1)}n_i - (\kappa_1+\kappa_2)\frac{\partial \bar{v}_{V|j}^{(1)}n_j}{\partial y} - g_2\frac{\partial \bar{v}_{V|j}^{(1)}t_j^1}{\partial y} - \frac{1}{h_1}\frac{\partial}{\partial \chi_1}\left(\frac{\partial \bar{v}_{V|j}^{(1)}t_j^1}{\partial y}\right) + g_1\frac{\partial \bar{v}_{V|j}^{(1)}t_j^2}{\partial y} - \frac{1}{h_2}\frac{\partial}{\partial \chi_2}\left(\frac{\partial \bar{v}_{V|j}^{(1)}t_j^2}{\partial y}\right), \tag{C3a}$$

$$\frac{\partial \bar{v}_{V|j}^{(2)}n_j}{\partial y} = i\zeta\sigma_V^{(1)} - (\kappa_1+\kappa_2)\bar{v}_{V|j}^{(1)}n_j - g_2\bar{v}_{V|j}^{(1)}t_j^1 - \frac{1}{h_1}\frac{\partial \bar{v}_{V|j}^{(1)}t_j^1}{\partial \chi_1} + g_1\bar{v}_{V|j}^{(1)}t_j^2 - \frac{1}{h_2}\frac{\partial \bar{v}_{V|j}^{(1)}t_j^2}{\partial \chi_2} + y\left(-g_2\frac{\partial \bar{v}_{V|j}^{(0)}t_j^1}{\partial y} - \frac{1}{h_1}\frac{\partial}{\partial \chi_1}\left(\frac{\partial \bar{v}_{V|j}^{(0)}t_j^1}{\partial y}\right) + g_1\frac{\partial \bar{v}_{V|j}^{(0)}t_j^2}{\partial y} - \frac{1}{h_2}\frac{\partial}{\partial \chi_2}\left(\frac{\partial \bar{v}_{V|j}^{(0)}t_j^2}{\partial y}\right)\right), \tag{C3b}$$

$$\begin{aligned}
\frac{\partial^2 \bar{v}_{V|i}^{(2)}t_i^q}{\partial y^2} + 2i\zeta\bar{v}_{V|i}^{(2)}t_i^q = {} & -\frac{1}{h_q}\frac{\partial}{\partial \chi_q}\left(\frac{\partial \bar{v}_{V|j}^{(1)}n_j}{\partial y}\right) + \frac{1}{h_q}\frac{\partial P_V^{(2)}}{\partial \chi_q} - \\
& \frac{2i\zeta}{h_q}\frac{\partial \tau_V^{(0)}}{\partial \chi_q} - \frac{\partial \bar{v}_{V|i}^{(1)}t_i^q}{\partial y}(\kappa_1+\kappa_2) - \bar{v}_{V|i}^{(0)}n_i(g_{3-q}-g_q)(\kappa_1-\kappa_2) + \\
& \bar{v}_{V|i}^{(0)}t_q^1\left(g_q^2 + 2g_{3-q}^2 + 2\kappa_q^2 + \kappa_1\kappa_2 + g_1g_2 - \frac{(-1)^{q+1}}{h_{3-q}}\frac{\partial g_q}{\partial \chi_{3-q}}\right) + \\
& \bar{v}_{V|i}^{(0)}t_i^{3-q}\left(\frac{2(-1)^{q+1}}{h_q}\frac{\partial g_q}{\partial \chi_q} + \frac{(-1)^{q+1}}{h_{3-q}}\frac{\partial g_{3-q}}{\partial \chi_{3-q}}\right) - \frac{1}{h_q}\frac{\partial \bar{v}_{V|i}^{(0)}n_i}{\partial \chi_q}(4\kappa_q+\kappa_{3-q}) - \\
& \frac{\partial \bar{v}_{V|i}^{(0)}t_i^q}{\partial \chi_q}\left(\frac{2}{h_q}\frac{\partial}{\partial \chi_q}\left(\frac{1}{h_q}\right) + \frac{2(-1)^{q+1}g_{3-q}}{h_q}\right) + \frac{3(-1)^{q+1}g_q}{h_q}\frac{\partial \bar{v}_{V|i}^{(0)}t_i^{3-q}}{\partial \chi_q} - \frac{(-1)^{q+1}}{h_{3-q}}\frac{\partial}{\partial \chi_{3-q}}\left(\frac{1}{h_{3-q}}\right)\frac{\partial \bar{v}_{V|i}^{(0)}t_i^q}{\partial \chi_{3-q}} + \\
& \frac{3(-1)^{q+1}g_{3-q}}{h_{3-q}}\frac{\partial \bar{v}_{V|i}^{(0)}t_i^{3-q}}{\partial \chi_{3-q}} - \frac{1}{h_1h_2}\frac{\partial}{\partial \chi_{3-q}}\left(\frac{\partial \bar{v}_{V|i}^{(0)}t_i^{3-q}}{\partial \chi_q}\right) - \frac{1}{h_{3-q}}\frac{\partial}{\partial \chi_{3-q}}\left(\frac{1}{h_{3-q}}\frac{\partial \bar{v}_{V|i}^{(0)}t_i^q}{\partial \chi_{3-q}}\right) + \frac{15i\zeta}{8h_q}\frac{\partial P_V^{(0)}}{\partial \chi_q} + \\
& i\zeta\frac{\partial^2 \bar{v}_{V|i}^{(0)}t_i^q}{\partial y^2} - \left(n_i\frac{\partial}{\partial x_i}\left(\frac{1}{h_q}\right)\right)_0\left(\frac{\partial \bar{v}_{V|j}^{(0)}n_j}{\partial \chi_q} + h_q\kappa_1\frac{\partial}{\partial y}\left(y\bar{v}_{V|j}^{(0)}t_j^q\right)\right) + \\
& y\left(n_i\frac{\partial}{\partial x_i}\left(\frac{1}{h_q}\right)\right)_0\left(\frac{\partial P_V^{(1)}}{\partial \chi_q} - \frac{\partial \bar{v}_{V|i}^{(0)}t_i^q}{\partial y}h_q(2\kappa_q+\kappa_{3-q})\right) + \\
& \frac{1}{2}\left(\left[n_i\frac{\partial}{\partial x_i}\right]^2\left(\frac{1}{h_q}\right)\right)_0\frac{\partial P_V^{(0)}}{\partial \chi_q} - y^2t_i^q\zeta\left(\frac{\partial^2 a_i}{\partial r^2}\right)_0,
\end{aligned} \tag{C3c}$$

$$\begin{aligned}
\frac{\partial^2 \tau_V^{(2)}}{\partial y^2} + 2i\zeta\tau_V^{(2)} = {} & \frac{4}{5}i\zeta P_V^{(2)} + \frac{11}{5}i\zeta\frac{\partial^2 \tau_V^{(0)}}{\partial y^2} - \\
& \left(2\zeta a_{i,0}n_i + \frac{\partial \tau_V^{(1)}}{\partial y} + y\left(n_i\frac{\partial}{\partial x_i}\left(\frac{1}{h_1}\right)\right)_0 h_1\frac{\partial \tau_V^{(0)}}{\partial y}\right)(\kappa_1+\kappa_2) - \\
& 2\zeta a_it_i^1g_2 - \frac{2\zeta}{h_1}\frac{\partial}{\partial \chi_1}\left(a_it_i^1\right) - \frac{2\zeta}{h_2}\frac{\partial}{\partial \chi_2}\left(a_it_i^2\right) + \frac{g_1}{h_2}\frac{\partial P_V^{(0)}}{\partial \chi_2} - \\
& \frac{1}{h_1h_2}\left(\frac{\partial}{\partial \chi_1}\left(\frac{h_2}{h_1}\frac{\partial}{\partial \chi_1}\right) + \frac{\partial}{\partial \chi_2}\left(\frac{h_1}{h_2}\frac{\partial}{\partial \chi_2}\right)\right)\left(\tau_V^{(0)}\right).
\end{aligned} \tag{C3d}$$

[1] F. Vuillot and G. Avalon, "Acoustic boundary layers in solid propellant rocket motors using Navier-Stokes equations," Journal of Propulsion and Power, vol. 7, pp. 231–239, 1991.

[2] A. Kierkegaard, S. Boij, and G. Efraimsson, "A frequency domain linearized Navier–Stokes equations approach to acoustic propagation in flow ducts with sharp edges," The Journal of the Acoustical Society of America, vol. 127, pp. 710–719, 2010.

[3] M. E. Berkman, L. N. Sankar, C. R. Berezin, and M. S. Torok, "Navier-Stokes/full potential/free-wake method for rotor flows," Journal of Aircraft, vol. 34, pp. 635–640, 1997.

[4] D.-Y. Shin, P. Grassia, and B. Derby, "Oscillatory limited compressible fluid flow induced by the radial motion of a thick-walled piezoelectric tube," The Journal of the Acoustical Society of America, vol. 114, pp. 1314–1321, 2003.

[5] L. Selle, L. Benoit, T. Poinsot, F. Nicoud, and W. Krebs, "Joint use of compressible large-eddy simulation and Helmholtz solvers for the analysis of rotating modes in an industrial swirled burner," Combustion and Flame, vol. 145, pp. 194–205, 2006.

[6] R. Erdélyi and V. Fedun, "Magneto-acoustic waves in compressible magnetically twisted flux tubes," Solar Physics, vol. 263, pp. 63–85, 2010.

[7] M. M. Abdel-Jawad, M. J. Goldsworthy, and M. N. Macrossan, "Stability analysis of Beagle 2 in the free-molecular and transition regimes," Journal of Spacecraft and Rockets, vol. 45, pp. 1207–1212, 2008.

[8] R. Lyle, P. Stabekis, L. Sentman, and R. Passamaneck, "Spacecraft aerodynamic torques," NASA SP-8058, 1971.

[9] M. Defoort, K. Lulla, T. Crozes, O. Maillet, O. Bourgeois, and E. Collin, "Slippage and boundary layer probed in an almost ideal gas by a nanomechanical oscillator," Physical Review Letters, vol. 113, p. 136101, 2014.

[10] M. Li, H. X. Tang, and M. L. Roukes, "Ultra-sensitive NEMS-based cantilevers for sensing, scanned probe and very high-frequency applications," Nature Nanotechnology, vol. 2, p. 114, 2007.

[11] P. L. Bhatnagar, E. P. Gross, and M. Krook, "A model for collision processes in gases. i. small amplitude processes in charged and neutral one-component systems," Physical Review, vol. 94, p. 511, 1954.

[12] P. Welander, "On the temperature jump in a rarefied gas," Arkiv Fysik, vol. 7, 1954.

[13] C. Cercignani, Rarefied Gas Dynamics: from basic concepts to actual calculations, vol. 21. Cambridge University Press, 2000.

[14] G. Bird, "Approach to translational equilibrium in a rigid sphere gas," Physics of Fluids, vol. 6, pp. 1518–1519, 1963.

[15] G. A. Bird and J. Brady, Molecular Gas Dynamics and the Direct Simulation of Gas Flows, vol. 5. Clarendon Press Oxford, 1994.

[16] N. G. Hadjiconstantinou, A. L. Garcia, M. Z. Bazant, and G. He, "Statistical error in particle simulations of hydrodynamic phenomena," Journal of Computational Physics, vol. 187, pp. 274–297, 2003.

[17] J. Chun and D. Koch, "A direct simulation Monte Carlo method for rarefied gas flows in the limit of small Mach number," Physics of Fluids, vol. 17, p. 107107, 2005.

[18] D. R. Ladiges and J. E. Sader, "Frequency-domain deviational Monte Carlo method for linear oscillatory gas flows," Physics of Fluids, vol. 27, p. 102002, 2015.

[19] D. R. Ladiges and J. E. Sader, "Frequency-domain Monte Carlo method for linear oscillatory gas flows," Journal of Computational Physics, vol. 284, pp. 351–366, 2015.

[20] C. Cercignani, "A variational principle for boundary value problems in kinetic theory," Journal of Statistical Physics, vol. 1, pp. 297–311, 1969.

[21] D. R. Ladiges and J. E. Sader, "Variational method enabling simplified solutions to the linearized Boltzmann equation for oscillatory gas flows," Physical Review Fluids, vol. 3, p. 053401, 2018.

[22] C. Cercignani, "Higher order slip according to the linearized Boltzmann equation," tech. rep., California Univ Berkeley Inst of Engineering Research, 1964.

[23] H. Grad, "On the kinetic theory of rarefied gases," Communications on Pure and Applied Mathematics, vol. 2, pp. 331–407, 1949.

[24] C. D. Levermore, "Moment closure hierarchies for kinetic theories," Journal of Statistical Physics, vol. 83, pp. 1021–1065, 1996.

[25] C. P. Groth and J. G. McDonald, "Towards physically realizable and hyperbolic moment closures for kinetic theory," Continuum Mechanics and Thermodynamics, vol. 21, pp. 467–493, 2009.

[26] H. Struchtrup, "The BGK-model with velocity-dependent collision frequency," Continuum Mechanics and Thermodynamics, vol. 9, pp. 23–31, 1997.

[27] H. Struchtrup, "Kinetic schemes and boundary conditions for moment equations," Zeitschrift für Angewandte Mathematik und Physik ZAMP, vol. 51, pp. 346–365, 2000.

[28] D. Hilbert, "Grundzüge einer allgemeinen theorie der linearen integralgleichungen. vierte mitteilung," Nachrichten von der Gesellschaft der Wissenschaften zu Göttingen, Mathematisch-Physikalische Klasse, vol. 1906, pp. 157–228, 1906.

[29] M. Lighthill, "A new approach to thin aerofoil theory," The Aeronautical Quarterly, vol. 3, pp. 193–210, 1951.

[30] C. Cercignani, "Elementary solutions of the linearized gas-dynamics Boltzmann equation and their application to the slip-flow problem," Annals of Physics, vol. 20, pp. 219–233, 1962.

[31] Y. Sone, "Asymptotic theory of flow of rarefied gas over a smooth boundary II," Rarefied Gas Dynamics, pp. 737–749, 1971.

[32] Y. Sone, Molecular Gas Dynamics: Theory, Techniques, and Applications. Springer Science & Business Media, 2007.

[33] Y. Sone, C. Bardos, F. Golse, and H. Sugimoto, "Asymptotic theory of the Boltzmann system, for a steady flow of a slightly rarefied gas with a finite Mach number: General theory," European Journal of Mechanics-B/Fluids, vol. 19, pp. 325–360, 2000.

[34] J. Nassios and J. E. Sader, "Asymptotic analysis of the Boltzmann–BGK equation for oscillatory flows," Journal of Fluid Mechanics, vol. 708, pp. 197–249, 2012.

[35] S. Takata and M. Hattori, "Asymptotic theory for the time-dependent behavior of a slightly rarefied gas over a smooth solid boundary," Journal of Statistical Physics, vol. 147, pp. 1182–1215, 2012.

[36] J. Nassios and J. E. Sader, "High frequency oscillatory flows in a slightly rarefied gas according to the Boltzmann–BGK equation," Journal of Fluid Mechanics, vol. 729, pp. 1–46, 2013.

[37] Y. Sone, "Asymptotic theory of flow of rarefied gas over a smooth boundary I," Rarefied Gas Dynamics, pp. 243–253, 1969.

[38] N. G. Hadjiconstantinou, "Comment on Cercignani's second-order slip coefficient," Physics of Fluids, vol. 15, pp. 2352–2354, 2003.

[39] S. Chapman, "On the law of distribution of molecular velocities, and on the theory of viscosity and thermal conduction, in a non-uniform simple monatomic gas," Philosophical Transactions of the Royal Society of London. Series A, Containing Papers of a Mathematical or Physical Character, vol. 216, pp. 279–348, 1916.

[40] D. Enskog, "Kinetische Theorie der Vorgänge in mässig verdünnten Gasen. I. Allgemeiner Teil," 1917.

[41] K. Aoki, C. Baranger, M. Hattori, S. Kosuge, G. Martalo, J. Mathiaud, and L. Mieussens, "Slip boundary conditions for the compressible Navier–Stokes equations," Journal of Statistical Physics, vol. 169, pp. 744–781, 2017.

[42] N. Z. Liu, "Transport equations and boundary conditions for oscillatory rarefied gas flows," Master's thesis, The University of Melbourne, https://minerva-access.unimelb.edu.au/handle/11343/224064, 2018.

[43] M. Hattori and S. Takata, "Sound waves propagating in a slightly rarefied gas over a smooth solid boundary," Physical Review Fluids, vol. 4, p. 103401, 2019.

[44] W. G. Vincenti and C. H. J. Kruger, Introduction to Physical Gas Dynamics. 8th edition, Krieger, 1965.

[45] We assume that this body force is independent of the particle velocity.

[46] H. Cartan, Course de Calcul Differentiel. Hermann, 1977.

[47] Y. Sone and Y. Onishi, "Kinetic theory of evaporation and condensation," Journal of the Physical Society of Japan, vol. 35, pp. 1773–1776, 1973.

[48] C. Bardos, R. E. Caflisch, and B. Nicolaenko, "The Milne and Kramers problems for the Boltzmann equation of a hard sphere gas," Communications on Pure and Applied Mathematics, vol. 39, pp. 323–352, 1986.

[49] Y. Sone, "Kinetic theory analysis of linearized Rayleigh problem," Journal of the Physical Society of Japan, vol. 19, pp. 1463–1473, 1964.

[50] A. Sommerfeld, "Die Greensche funktion der schwingungsgleichung," J.-Ber. Deutsch Math.-Verein, vol. 21, pp. 309–353, 1912.

[51] A. Manela and N. G. Hadjiconstantinou, "Gas motion induced by unsteady boundary heating in a small-scale slab," Physics of Fluids, vol. 20, p. 117104, 2008.

[52] A. Manela and N. G. Hadjiconstantinou, "Gas-flow animation by unsteady heating in a microchannel," Physics of Fluids, vol. 22, p. 062001, 2010.

[53] J. Nassios, Y. W. Yap, and J. E. Sader, "Flow generated by oscillatory uniform heating of a rarefied gas in a channel," Journal of Fluid Mechanics, vol. 800, pp. 433–483, 2016.

[54] D. R. Ladiges, Oscillatory rarefied flows: Monte Carlo and variational methods. PhD thesis, The University of Melbourne, 2016.

[55] Y. W. Yap and J. E. Sader, "Sphere oscillating in a rarefied gas," Journal of Fluid Mechanics, vol. 794, pp. 109–153, 2016.

[56] M. Abramowitz and I. A. Stegun, Handbook of Mathematical Functions: with Formulas, Graphs, and Mathematical Tables, vol. 55. Courier Corporation, 1965.